Research Paper

Paleocene–early Eocene post-subduction magmatism in Sikhote-Alin (Far East Russia): New constraints for the tectonic history of the Izanagi-Pacific ridge and the East Asian continental margin

Andrei V. Grebennikov [a,*], Igor V. Kemkin [a], Alexander I. Khanchuk [a,b]

[a] *Far East Geological Institute, Far Eastern Branch, Russian Academy of Sciences, pr. 100-letiya Vladivostok 159, Vladivostok 690022, Russia*
[b] *Institute of Geology of Ore Deposits, Petrography, Mineralogy and Geochemistry (IGEM), Russian Academy of Sciences, 35 Staromonetny Per., Moscow 109017, Russia*

A B S T R A C T

New isotopic, geochemical and geochronological data justify the widespread occurrence of middle Paleocene to early Eocene (60–53 Ma) post-subduction felsic magmatism across the entire Sikhote-Alin territory (southeastern Russia), conform with previous observations in Northeast China, the southern Korean Peninsula, and the Inner Zone of Japan. This igneous activity in East Asia coincided with the reactivation (after tectonic quiescence between ~93–60 Ma) of left-lateral strike-slip displacements along the Tan-Lu and Central Sikhote-Alin faults and with the post-60 Ma cessation of subduction/accretion recorded in the Shimanto belt of SW Japan. The Sikhote-Alin post-subduction igneous A-type rocks present diverse mineralogical and geochemical features that suggest interactions of the subducting plate with anhydrous mantle upwelling through slab tears in the continental margin. The middle Paleocene–early Eocene magmatism is not related to subduction but is synchronous with strike-slip tectonics and the termination of accretionary prism development, suggesting a shift in tectonic regime from oceanic plate subduction at a convergent margin to parallel sliding and initiation of a transform continental margin. These new observations are inconsistent with the current tectonic model of 60–50 Ma Izanagi-Pacific ridge subduction beneath East Asian continental margin.

1. Introduction

In recent years, the Pacific margin of East Asia has attracted research attention because it is a potential source of various geological information for developing geodynamic evolution models of the paleo-Asian continental margin in the Mesozoic–Cenozoic and clarifying the reasons for changes in the kinematics of the relative motion of the Pacific Plate (e.g., Nokleberg et al., 2000; Khanchuk, 2006; Seton et al., 2015; Domeier et al., 2017; Kimura et al., 2019; Vaes et al., 2019; Wu and Wu, 2019). One of the controversial problems touches upon the character of plate interactions at the beginning of the Paleogene in East Asia. A prevailing idea indicates that continuous subduction occurred during the Late Cretaceous–Paleogene (e.g., Maruyama et al., 1997; Jahn et al., 2015; Müller et al., 2016; Tang et al., 2016; Zhao et al., 2017). As subduction cessation occurred at the beginning of the Paleogene, East Asia changed from an Andean-type convergent margin to a California-type transform margin (Khanchuk, 2001, 2006; Grebennikov et al., 2016; Martynov et al., 2017).

Another debatable point arises from plate tectonic reconstructions of the assumed Izanagi-Pacific ridge subduction between 60 and

50 Ma, which was subparallel to a large swath of the northeastern Asian margin (e.g., Whittaker et al., 2007; Seton et al., 2015), and its possible geological indicators. Based on a magmatic gap, researchers have distinguished indicators that include intense subduction erosion and forearc thermal events in the Shimanto belt, back-arc thermal events and extensive unconformities in the Songliao Basin between 56 and 46 Ma (Wu and Wu, 2019), while others distinguished indicators in the Paleocene gap based on the formation of an accretionary prism in the Shimanto belt and the inferred absence of magmatism synchronous with these events in Japan (e.g., Kimura et al., 2019).

Compared with Japan, the territory of the Sikhote-Alin contains the products of Paleocene magmatism; these products are synchronous with the suggested time of Izanagi-Pacific ridge subduction and widely distributed (Fig. 1), and they have mineralogical and geochemical features inherent to A-type igneous rocks (Grebennikov and Maksimov, 2006, 2021; Grebennikov and Popov, 2014; Jahn et al., 2015; Grebennikov et al., 2016). These features are typical for the mantle and crustal magmatism of extensional zones, and they cannot be realized in an orthogonal or oblique subduction setting that determines the compressional conditions at a convergent margin. This contradiction is probably why researchers who support the continuous subduction model during the Cretaceous–early Paleogene geodynamic evolution of the paleo-Asian eastern margin prefer to suppress the
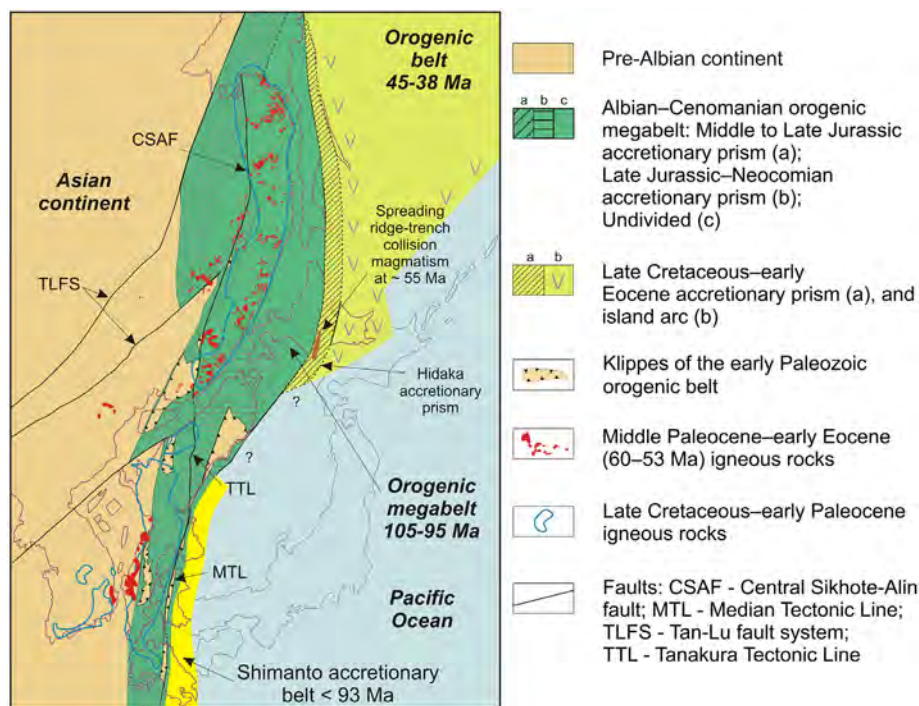
Fig. 1. Paleotectonic reconstruction of East Asia before the formation of the Sea of Japan. The position of Japan before the opening of the Sea of Japan is reconstructed based on Khanchuk (2001) and Kemkin et al. (2016).

existence of Paleocene A-type igneous rocks that are "so inconvenient" for their models or suggest that this problem will be resolved in future publications (Jahn et al., 2015; Tang et al., 2016; Zhao et al., 2017, etc.).

In this paper, we present new data for the middle Paleocene to early Eocene (60.5–53 Ma) igneous rocks within the territory of the Sikhote-Alin orogenic belt (southeastern Russia) and their correlation with the same types of rocks in East Asia. These data along with the authors' geological review are inconsistent with the widespread interpretation of Izanagi-Pacific ridge subduction at this time.

2. Brief geological background of the Sikhote-Alin orogenic belt

The Sikhote-Alin–West Sakhalin orogenic belt (herein referred to as the Sikhote-Alin) of the Russian Far East represents the southern part of the late Albian–Cenomanian orogenic megabelt of Pacific Asia (Khanchuk et al., 2019, and references therein). It extends along a strip with a northeastern strike from the northern coast of the Sea of Japan to the lower reaches of the Amur River and the western part of Sakhalin Island (Fig. 2) and is approximately 1500 km long and 600 km wide.

The belt is composed of several terranes, including deformed fragments of the Jurassic and Early Cretaceous accretionary wedges (Samarka, Nadanhada–Bikin, Khabarovsk, Badzhal, Taukha, and Kiselevka–Manoma), the Hauterivian to middle Albian island arc (Kema, and Shmidt and Kamyshov on Sakhalin Island), and the Early Cretaceous Zhuravlevka–Amur turbidite basin (Khanchuk, 2001; Kemkin, 2008; Kemkin et al., 2016; Khanchuk et al., 2016). These Mesozoic terranes overlap with Turonian–Maastrichtian and Cenozoic undeformed volcanic rocks and sediments (Khanchuk, 2006; Grebennikov and Popov, 2014; Khanchuk et al., 2019, etc.). The Jurassic and Early Cretaceous accretionary prisms, such as the Early Cretaceous island arc, formed as a result of the subduction of the oceanic plate (Khanchuk, 2001; Kemkin, 2008; Kemkin et al., 2016; Khanchuk et al., 2016, etc.). The turbidite basin that started to form in the Valanginian was related to the sinistral sliding of the oceanic plate along the continental margin

(e.g., Golozubov and Khanchuk, 1995; Khanchuk, 2001, 2006; Kemkin et al., 2016; Khanchuk et al., 2016, etc.).

In the setting of transform interactions, a system of left-lateral strike-slip faults (the so-called Tan-Lu fault system) developed at the eastern margin of the paleo-Asian continent, and large-scale displacements occurred along these faults during the Neocomian–Albian accompanied by intense folding and thrusting. These deformations led to the formation of the Sikhote-Alin fold orogen. The intrusion of large volumes of Hauterivian–Aptian (130–120 Ma) and late Albian–early Cenomanian (110–98 Ma) granitoid magmas accounts for the occurrence of a granitic-metamorphic layer in the lower part of the orogen and hence completed the formation of the new block of continental lithosphere (Khanchuk et al., 2016). Before the opening of the Sea of Japan basin (15–17 Ma) (e.g., Otofuji and Matsuda, 1983, 1987; Otofuji et al., 1985, etc.), the Sikhote-Alin–West Sakhalin orogenic belt that consists of the Japanese Islands and part of the Ryukyu Islands stretched farther south (in modern coordinates). Except for the Zhuravlevka–Amur terrane, analogs of the Sikhote-Alin and Sakhalin terranes are sufficiently well studied within these territories (e.g., Taira and Tashiro, 1987; Kojima, 1989; Ichikawa et al., 1990; Mizutani and Kojima, 1992; Khanchuk, 2001; Taira, 2001; Kemkin, 2006; Moreno et al., 2016, and references therein). For example, the Sikhote-Alin terranes of the Jurassic accretionary prism can be compared to the Mino, Tamba, and Ashio terranes and their metamorphosed analog, namely, the Ryoke terrane in the Inner Zone of Japan. In the Outer Zone of Japan, their analogs are the Northern Chichibu terrane and the Jurassic part of the Sanbagawa terrane. The Sikhote-Alin fragment of the Late Jurassic–Early Cretaceous prism, i.e., the Taukha terrane, correlates with the Southern Chichibu, Ryukyu, Northern Kitakami, and Oshima terranes in the Outer Zone of Japan. The Rebun-Kabato terrane of Hokkaido together with the Kema terrane of the Sikhote-Alin and Kamyshov and Shmidt terranes of Sakhalin represent scattered fragments of the Early Cretaceous island arc.

Similar to the Sikhote-Alin, large-scale left-lateral strike-slip displacements of the terranes occurred within the Japanese Islands along the faults of the Median and Tanakura tectonic lines in the Albian are
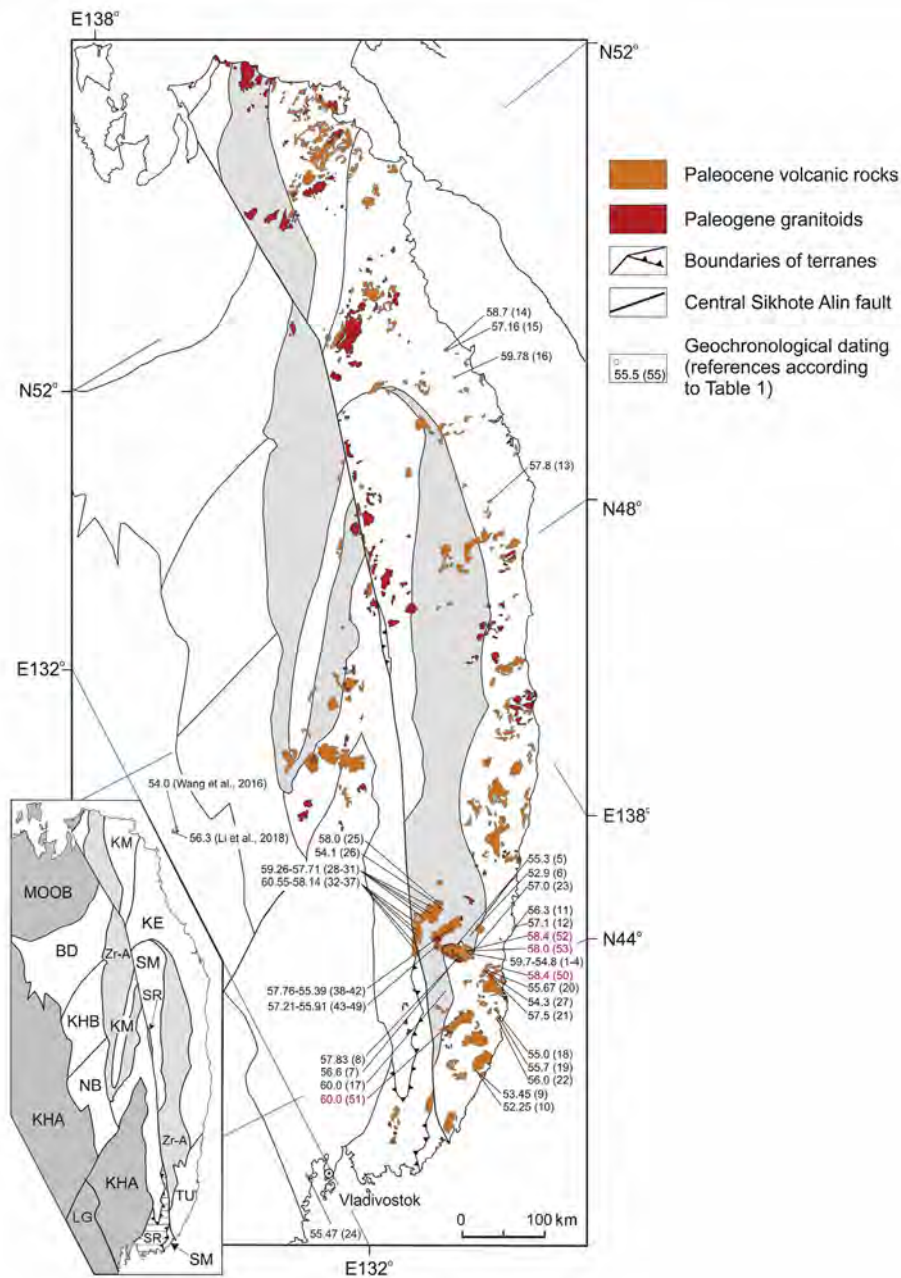
Fig. 2. Paleocene magmatic rocks from the Russian Far East and NE China. Inset: Terranes of the Middle–Late Jurassic accretionary wedge: (BD) Badzhal, (NB) Nadankhada–Bikin, (SM) Samarka and (KHB) Khabarovsk. Late Tithonian–Valanginian: (TU) Taukha. Barremian–early Albian: (KM) Kiselevka–Manoma. Barremian–early Albian island arc: (KE) Kema. Early Cretaceous turbidite basin: (Zr-A) Zhuravlevka–Amur. (SR) Sergeevka terrane of Paleozoic continental allochthons on the terrane of the Jurassic accretionary wedge; (KHA) Early Paleozoic Badzhal–Jiamusi–Khanka superterrane; (LG) Triassic Laoeling–Grodekovo terrane; and (MOOB) Jurassic Mongol–Okhotsk terrane of orogenic belts.

described and confirmed by the contrast of the pre-Albian flora between the boreal flora to the west and subtropical flora to the east of these faults as well as by structural observations (e.g., Moreno et al., 2016). This interpretation is also supported by observations of the Lower Cretaceous deposits that contain subtropical flora, which identified the presence of detrital zircon populations from the rocks of Southeast China but not from the rocks of the Inner Zone of Japan and Korea (Ikeda et al., 2016).

The Late Cretaceous–early Paleocene magmatic activity in the Sikhote-Alin was dominated by Andean-type convergent margin tectonics and magmatism, which are exemplified by the formation of the East Sikhote-Alin volcanic-plutonic belt (ESAVPB). This belt consists of a large volume of volcanic rocks overlying the Early Cretaceous Kema,

Taukha, and Zhuravlevka–Amur terranes (e.g., Sakhno, 2001; Khanchuk, 2006, and references therein). These volcanic rocks range in composition from andesitic to rhyolitic, and their emplacement has been dated to the latest Cenomanian–early Paleocene (Khanchuk, 2006; Jahn et al., 2015; Tsutsumi et al., 2016, etc.). Volcanic activity was accompanied by the emplacement of numerous granitoid plutons in the same areas. Their calc-alkaline, ferroan, and magnesian compositions correspond to metaluminous felsic magmas of mostly I-type. The formation of such melts is explained by the partial melting of metasedimentary and metaigneous rocks in a relatively oxidizing environment with water, which is typical for the volcanism of suprasubduction geodynamic settings (Khanchuk, 2006; Grebennikov and Popov, 2014; Jahn et al., 2015, etc.).

3

3. Middle Paleocene–early Eocene magmatism of the Sikhote-Alin

According to geological mapping, middle Paleocene–early Eocene felsic rocks are widely distributed throughout the entire Sikhote-Alin territory, along the Central Sikhote-Alin fault and along the adjacent end of the Tan-Lu fault system (see Fig. 2). To date, limited precise isotopic, geochemical and geochronological data on the late Paleocene granites of this region have been published, and incorrect conclusions regarding their supra-subduction nature have been drawn (Jahn et al., 2015; Tang et al., 2016; Zhao et al., 2017). In Table 1, we provide a selection of all up-to-date geochronological data that have been published on the Paleocene igneous rocks from the Russian Far East (see Fig. 2 and references therein for details).

These rocks are distinguished by the composition of rhyodacitic-rhyolitic and leucogranitic complexes, which form multiple volcanic depressions. Considering that erosion has reached the shallow magmatic

chambers, their size is 40 km × 20 km (e.g., Yakut volcanic depression, see Grebennikov and Maksimov, 2006), while the total volume of the Paleocene volcanic products greatly surpasses that of the Yellowstone caldera (see Grebennikov and Maksimov, 2021).

The facies diversity of pyroclastic rocks consists of various stages of the explosive process involved in ignimbrite formation. The rhyodacitic-rhyolitic ignimbrites and voluminous bodies of volcanic glasses contain large quantities of quartz, sanidine, albite-oligoclase, ferrohypersthene, ferrohedenbergite, ferroaugite, biotite, and fayalite. Dominating accessory minerals are orthite, ilmenite, zircon, apatite, native iron and cohenite (Fe_3C), which suggests a highly reduced primary melt composition (Grebennikov and Maksimov, 2006; Grebennikov, 2011; Grebennikov et al., 2012).

The granitoids are genetically related to the volcanic rocks, which explains why these intrusions are spatially limited to the volcanic fields of the East Sikhote-Alin area. The sheet-like granitoid bodies intrude

Table 1
Age data for the Paleocene magmatic rocks from the Russian Far East and NE China.

#	Rocks	Method	Localites	Age (Ma)	Sources
1	Ignimbrite	Rb–Sr	N44°30′39″, E135°21′31″	59.7 ± 1.6	Popov and Grebennikov, 2001;
2	Ignimbrite		N44°30′55″, E135°21′28″	58.0 ± 3.6	Grebennikov and Maksimov, 2006
3	Ignimbrite		N44°31′16″, E135°21′08″	56.3 ± 1.2	
4	Ignimbrite		N44°31′40″, E135°21′26″	54.8 ± 2.6	
5	Granite		N44°38′24″, E135°16′07″	55.3 ± 2.8	
6	Lava, perlite		N44°32′06″, E135°24′23″	52.9 ± 3.5	
7	Lava, dacite	U–Pb SHRIMP	N44°31′22″, E135°09′56″	56.6 ± 1.2	Alenicheva and Sakhno, 2008
8	Granite		N44°31′37″, E135°13′27″	57.83 ± 1.1	
9	Tuff, rhyolite	U–Pb SHRIMP	N43°21′51″, E134°34′18″	53.45 ± 0.5	Sakhno et al., 2010
10	Tuff, rhyolite		N43°21′51″, E134°34′18″	52.25 ± 0.43	
11	Q-monzodiorite	LA-ICP-MS	N44°30′04″, E136°10′13″	56.3 ± 0.7	Jahn et al., 2015
12	Granite		N44°29′17″, E136°07′29″	57.1 ± 0.4	
13	Granite		N49°20′33″, E137°37′26″	57.8 ± 1.1	
14	Granodiorite	U–Pb SHRIMP	N50°34′52″, E139°46′07″	58.7 ± 0.4	Petrov et al., 2015
15	Granite		N50°35′53″, E139°47′59″	57.16 ± 0.91	
16	Syenogranite		N50°05′54″, E139°48′36″	59.78 ± 0.62	
17	Tuff, rhyolite	LA-ICP-MS	N44°16′29″, E134°46′38″	60.0 ± 0.9	Tsutsumi et al., 2016
18	Tuff, rhyolite		N43°49′19″, E135°16′29″	55.0 ± 1.3	
19	Granite		N43°44′09″, E135°15′56″	55.7 ± 0.7	
20	Lava, perlite	LA-ICP-MS	N44°14′58″, E135°27′04″	55.67 ± 0.74	Pavlyutkin et al., 2016
21	Tuff, rhyolite		N44°15′24″, E135°26′25″	57.5 ± 1.5	
22	Monzogranite	LA-ICP-MS	N43°43′44″, E135°14′24″	56.0 ± 1.0	Tang et al., 2016
23	Tuff, rhyolite	LA-ICP-MS	N44°29′39″, E135°23′14″	57.0 ± 1.0	Zhao et al., 2017
24	Lava, rhyolite	LA-ICP-MS	N42°41′59″, E130°49′42″	55.47 ± 2.5	Popov et al., 2018
25	Tuff, rhyolite	U–Pb SHRIMP	N45°09′32″, E135°20′06″	58.0 ± 1.0	Sakhno and Kovalenko, 2018
26	Syenogranite	LA-ICP-MS	N45°06′39″, E135°20′33″	54.1 ± 2.7	
27	Tuff, rhyolite	LA-ICP-MS	N44°17′10″, E135°17′59″	54.3 ± 2.9	Grebennikov and Maksimov, 2021
28	Lava, rhyolite	LA-ICP-MS	N45°06′44″, E135°02′54″	58.12 ± 0.16	Grebennikov et al., 2020
29	Lava, rhyolite		N45°04′47″, E135°08′23″	58.62 ± 0.18	
30	Tuff, rhyolite		N45°06′15″, E135°11′51″	57.71 ± 0.54	
31	Tuff, rhyolite		N45°07′39″, E135°02′13″	59.26 ± 0.12	
32	Lava, rhyolite		N44°49′11″, E134°41′53″	58.14 ± 0.22	
33	Tuff, rhyolite		N44°49′01″, E134°43′25″	59.03 ± 0.18	
34	Lava, rhyolite		N45°00′36″, E135°50′22″	60.14 ± 0.38	
35	Lava, rhyolite		N44°54′20″, E134°42′37″	60.55 ± 0.10	
36	Ignimbrite		N45°05′05″, E134°52′12″	58.75 ± 0.23	
37	Ignimbrite		N45°03′08″, E134°54′14″	59.72 ± 0.41	
38	Lava, rhyolite		N44°45′12″, E134°55′45″	55.39 ± 0.28	
39	Monzodiorite		N44°47′21″, E135°04′02″	56.34 ± 0.32	
40	Granite		N44°48′33″, E135°01′10″	57.54 ± 0.31	
41	Tuff, rhyolite		N44°44′51″, E134°57′46″	57.16 ± 0.20	
42	Tuff, rhyodacite		N44°45′07″, E135°03′52″	57.76 ± 0.23	
43	Syenogranite		N44°49′36″, E135°01′09″	55.91 ± 0.41	
44	Granite		N44°51′55″, E135°01′22″	56.49 ± 0.30	
45	Lava, rhyolite		N44°50′16″, E135°13′17″	56.56 ± 0.32	
46	Lava, rhyolite		N44°49′52″, E135°25′37″	56.79 ± 0.30	
47	Lava, rhyolite		N44°51′46″, E135°01′16″	57.21 ± 0.30	
48	Tuff, rhyolite		N44°52′35″, E135°04′37″	56.16 ± 0.21	
49	Tuff, rhyolite		N44°50′19″, E135°19′08″	56.79 ± 0.29	
50	Tuff, rhyolite	U–Pb SHRIMP	N44°10′60″, E135°39′60″	58.4 ± 1.5	This study
51	Tuff, rhyolite		N43°58′60″, E134°50′60″	60.0 ± 2.0	
52	Ignimbrite		N44°31′60″, E135°20′60″	58.4 ± 1.0	
53	Tuff, rhyolite		N44°30′60″, E135°20′60″	58.0 ± 1.1	

between volcanic strata, thus sealing off volcanic conduits and dikes, and fill ring and radial faults within volcanic depressions. Almost all of these intrusions are associated with subvolcanic endocontact zones that contain highly porphyritic rocks with poorly crystallized felsic, spherulitic, or axiolitic textures. The rocks are primarily alkali feldspar granites and leucogranites, with rare aegirine-riebeckite granites, and quartz syenites. The first two types have phenocrysts that consist predominantly of oligoclase (up to 40% modal abundance), quartz, perthitic alkali feldspar, and hypersthene and rarely of magnetite, augite, hornblende, and biotite. The peralkaline granites are fine-grained, porphyritic, or pegmatitic rocks that contain variable proportions of quartz, alkali feldspar, albite, aegirine, and riebeckite. Accessory minerals are predominantly zircon, xenotime, and bastnaesite and more rarely columbite, chevkinite or orthite (Mikhailov, 1989; Grebennikov and Maksimov, 2006; Jahn et al., 2015, etc.).

To establish precise age limits for the middle Paleocene–early Eocene volcanism in the South Sikhote-Alin territory, we present new U–Pb zircon ages determined with a sensitive high-resolution ion microprobe (SHRIMP). The samples were collected from the tuffs and ignimbrites of the lowermost rhyodacitic-rhyolitic volcanic units (Fig. 3).

U–Pb zircon dating was performed using the SHRIMP-II system in the Center of Isotopic Research of FGBU VSEGEI (named after A.P.

Karpinsky (VSEGEI, Saint Petersburg)) via common methods. The results are presented in Table 2.

The majority of zircons are transparent and have grain sizes of 150–300 μm. The grains are euhedral and show oscillatory zones typical of a magmatic origin. The Th/U ratios of all zircon samples are in the range of 0.47–1.15, indicating a magmatic origin. The mean age of the obtained results is given in U–Pb concordia diagrams (Fig. 4). The obtained isotopic data and weighted average U–Pb ages (see Table 2) of the lowermost rhyodacitic-rhyolitic volcanic units (4 samples) are 60.5–58 Ma (middle Paleocene: Selandian). These new results together with the published data indicate that in the Sikhote-Alin territory, magmatism occurred predominantly at ~60.5–53 Ma, i.e., in the middle Paleocene–early Eocene (Table 1).

The analysis of the geochemical data confirmed by geochronological dating (published and authors' material) shows that the rocks from the Paleocene stage of magmatism are represented in the Sikhote-Alin by high-silica intrusive and volcanic rocks (Fig. 5). They typically have SiO_2 concentrations of 65–75 wt.% and up to 82 wt.% in the most felsic volcanic units. They are characterized by high alkali concentrations (6.8–10.5 wt.%) and extremely low CaO and MgO concentrations, which are reflected in their high to moderate potassium, high alumina, agpaitic and ferruginous compositions. Wide variations in large ion
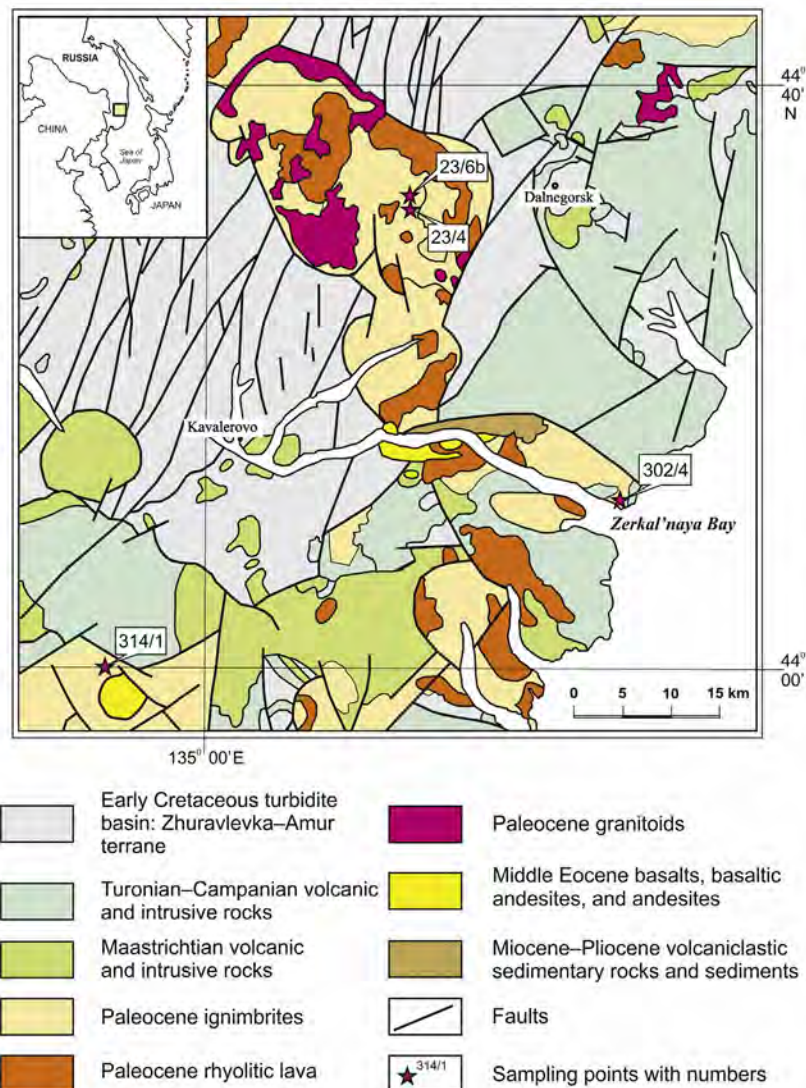
Fig. 3. Sketch map showing the distribution of Mesozoic–Cenozoic magmatic rocks in the southern Sikhote-Alin (Primorye) area of Far East Russia.

Table 2
LA-ICP-MS (Sensitive high-resolution ion microprobe) zircon U–Pb data.

Spot	$^{206}Pb_c$(%)	U(ppm)	Th(ppm)	$^{232}Th/^{238}U$	$^{206}Pb^*$(ppm)	$^{238}U/^{206}Pb$	$^{207}Pb/^{206}Pb$	$^{206}Pb/^{238}U$
23/4 (Mean age = 58.0 ± 1.1 Ma; Tuff, rhyolite; N44°31′, E135°21′)								
23/4.1.1	3.09	186	214	1.19	1.49	107.0 ± 2.9	0.0753 ± 7.1	58 ± 2.5
23/4.2.1	1.10	495	533	1.11	3.91	108.7 ± 2.3	0.0623 ± 4.7	58 ± 1.5
23/4.3.1	2.88	149	70	0.49	1.24	103.4 ± 3.1	0.0841 ± 7.6	60 ± 2.6
23/4.1.2	10.69	201	231	1.19	1.67	103.5 ± 3.1	0.0882 ± 6.1	55 ± 3.2
23/4.4.1	4.35	205	157	0.79	1.76	100.3 ± 2.8	0.1190 ± 5.4	61 ± 3.2
23/4.5.1	7.12	207	156	0.78	1.67	106.6 ± 2.8	0.0803 ± 7	56 ± 3.2
23/4.6.1	10.27	139	72	0.54	1.13	105.5 ± 3.2	0.0900 ± 12	55 ± 4
23/4.7.1	2.93	376	242	0.66	2.97	108.7 ± 2.5	0.0633 ± 7.3	57 ± 2.2
23/4.7.2	6.00	60	29	0.51	0.481	107.3 ± 4.4	0.1190 ± 10	56 ± 3.4
23/4.8.1	3.34	205	105	0.53	1.60	110.4 ± 2.9	0.0763 ± 6.3	56 ± 2.1
23/6b (Mean age = 58.4 ± 1.0 Ma; ignimbrite; N44°32′, E135°21′)								
23/6.1.1	1.68	1341	1225	0.94	10.5	109.8 ± 2.7	0.057 ± 4.3	57.4 ± 1.6
23/6.1.2	0.30	1362	1271	0.96	10.7	109.4 ± 2.7	0.057 ± 4.2	58.5 ± 1.6
23/6.2.1	1.90	912	660	0.75	7.4	105.9 ± 2.8	0.0647 ± 9.8	59.5 ± 1.8
23/6.3.1	3.27	1270	1078	0.88	9.98	109.3 ± 2.7	0.0599 ± 8	56.8 ± 1.8
23/6.4.1	1.84	1605	1403	0.90	12.8	107.3 ± 2.6	0.0554 ± 4	58.7 ± 1.7
23/6.5.1	1.56	1842	2113	1.19	14.8	106.7 ± 2.6	0.0567 ± 3.7	59.2 ± 1.6
23/6.6.1	1.71	1563	1478	0.98	12.3	109.3 ± 2.6	0.0559 ± 4	57.7 ± 1.6
23/6.7.1	1.39	1564	1965	1.30	12.6	106.4 ± 2.6	0.0558 ± 4	59.5 ± 1.6
23/6.8.1	0.89	1560	1343	0.89	12.3	108.7 ± 2.6	0.0571 ± 4	58.5 ± 1.6
23/6.9.1	1.62	1680	1470	0.90	13.5	106.9 ± 2.6	0.0625 ± 3.7	59 ± 1.6
302/4 (Mean age = 58.4 ± 1.5 Ma; Lava, rhyolite; N44°11′, E135°40′)								
302/4.1.1	4.33	199	134	0.70	1.64	104.2 ± 4	0.118 ± 15	58.9 ± 3.5
302/4.2.1	17.75	194	120	0.64	1.71	97.6 ± 4	0.1188 ± 8.2	54 ± 5.9
302/4.3.1	9.74	208	113	0.56	1.78	100.8 ± 3.9	0.0922 ± 10	57.4 ± 6.3
302/4.4.1	21.08	211	171	0.84	1.89	95.8 ± 3.8	0.1173 ± 8	52.8 ± 5.2
302/4.5.1	18.56	347	167	0.50	3.08	96.8 ± 3.4	0.147 ± 12	53.9 ± 6.5
302/4.6.1	2.75	208	174	0.86	1.79	99.9 ± 3.9	0.127 ± 8.4	62.4 ± 3
302/4.7.1	3.06	235	189	0.83	1.96	102.8 ± 4.2	0.115 ± 17	60.5 ± 2.8
302/4.8.1	12.22	594	351	0.61	5.14	99.3 ± 3.2	0.1257 ± 4.6	56.7 ± 3.1
3024.9.1	37.36	571	319	0.58	7.01	69.9 ± 2.9	0.3465 ± 2.8	57.3 ± 4.9
314/1 (Mean age = 60.0 ± 2.0 Ma; Tuff, rhyolite; N43°59′, E134°51′)								
314/1.5.1	0.28	79	82	1.06	0.58	117.9 ± 7.8	0.11 ± 24	54 ± 4.2
314/1.3.1	0.61	1617	962	0.61	12.20	113.9 ± 2.4	0.0518 ± 5.7	56 ± 1.4
314/1.2.1	4.99	110	94	0.88	0.91	104.1 ± 4.5	0.092 ± 12	59 ± 3.6
314/1.4.1	2.18	681	793	1.20	5.62	104.1 ± 2.2	0.0604 ± 4	60 ± 1.6
314/1.10.1	4.25	132	93	0.73	1.13	99.8 ± 3.2	0.101 ± 11	62 ± 3.1
314/1.6.1	2.74	262	329	1.30	2.25	100 ± 2.7	0.0746 ± 7.1	62 ± 2.3
314/1.8.1	6.30	46	43	0.98	0.42	94 ± 4.8	0.16 ± 20	64 ± 4.1
314/1.7.1	11.93	79	45	0.59	0.78	86.2 ± 3.8	0.184 ± 8.6	65 ± 5.1
314/1.9.1	4.44	86	68	0.82	0.84	87.8 ± 3.6	0.105 ± 17	70 ± 3.3
314/1.1.1	0.00	72	51	0.73	0.74	83.8 ± 6.4	0.075 ± 21	77 ± 4.9

lithophile elements (LILEs: K, Rb, Cs, Sr and Ba) and high concentrations of high field strength elements (HFSEs: Zr, Nb, Ga and Y) and rare earth elements (REEs) (except for Eu) are also typical of these rocks. The calculated T_{Zr} values are predominantly more than 800 °C, suggesting that the primary melts had a high temperature. In the multicomponent diagrams, the chondrite-normalized compositions of the rocks are similar to the REE spectra and show insignificant enrichments in light REEs (LREEs)/heavy REEs (HREEs) (3.5–10.5), low (La/Yb)$_N$ ratios (0.9 or 2.2–10.6) and negative Eu anomalies. In the spider diagrams of the primitive mantle-normalized trace elements, the rocks show negative Ba, Sr, and Ti; positive K, Th, U, and Pb; and weakly positive Ce, Zr, and Hf anomalies (Fig. 6); i.e., they exhibit geochemical characteristics typical of A-type igneous rocks but not highly fractionated granites. Their position in the discriminant diagrams indicates the same interpretation (Whalen et al., 1987; Frost et al., 2001; Dall'Agnol and De Oliveira, 2007; Grebennikov, 2014; Fig. 7). The occurrence of middle Paleocene–early Eocene magmatism can be confirmed via data on detrital zircons collected from Eocene and Miocene rock suites of the West Sakhalin (Malinovsky, 2019). Approximately 50% of the detrital zircons in sandstones of the Eocene suite are aged to the Paleocene–Eocene (47–65 Ma) and 36% are aged to the Late Cretaceous (69–99 Ma). Most zircon grains in sandstones of the Miocene suite are also of

Paleocene–Eocene (46–64 Ma, 25%) and Cretaceous (69–106 Ma, 30%) age. The other portion of zircon grains are characterized by a Paleozoic and Mesozoic age. Similar results (48–60 Ma and 64–106 Ma) were obtained in U–Pb age investigations of zircons from Miocene deposits in the southern area of West Sakhalin (Zhao et al., 2017).

4. Middle Paleocene–early Eocene igneous rocks of East Asia

Middle Paleocene–early Eocene igneous rocks that are analogous or close in their petro-geochemical characteristics to the rocks of the Sikhote-Alin are also distributed in the territories adjacent to the Sikhote-Alin. Recently, Li et al. (2018) reported that the late Paleocene–early Eocene granitoids in the Jiamusi Massif were emplaced at 56–52 Ma, thus representing the youngest granitic magmatism in NE China. Eocene granodiorites with a weighted average age of 54.0 ± 1.0 Ma have also been reported for the Sanjiang Basin (SW of the Sikhote-Alin) (Wang et al., 2016). South of the Sikhote-Alin in the Yanji area, NE China, Paleocene (ca. 58–55 Ma) adakitic andesites that are thought to have formed during post-subduction extension have been described. Paleocene tholeiitic to calc-alkaline basalts erupted in fault-rift basins around the Bohai Bay area and along the Tan-Lu fault
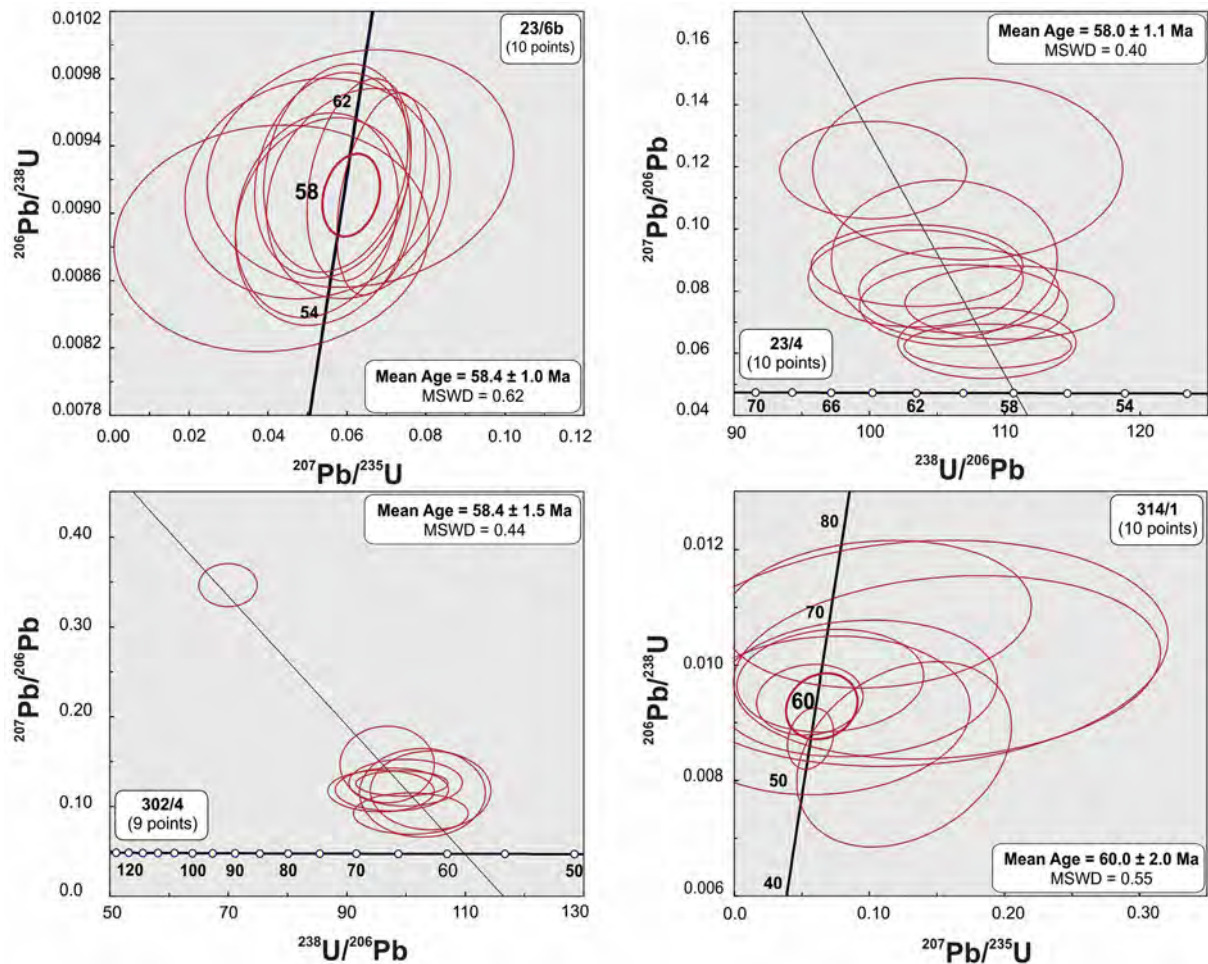
Fig. 4. U–Pb concordia diagrams for the Paleocene magmatic rocks from the Russian Far East.

system in response to lithospheric extension, suggesting a similar extensional regime (Guo et al., 2007, and references therein).

In the territory of Korea, middle Paleocene–early Eocene granites are found along the Korean east coast (SE Korean Peninsula) in the Gyeongsang basin. These are granodiorites and granites in the Gyeongju area on the east side of the Yangsan fault (54.0 ± 0.4 Ma; 36°06′N, 129°15′E), the Daejeonri pluton (57.5 ± 0.5 Ma; ~35°28′N, 129°18′E), and the Hoam pluton (50.8 ± 0.4 Ma; ~35°52′N, 129°18′E) (e.g., Hwang et al., 2012; Cheong et al., 2013). Their genesis is directly related to the onset of tectonic setting changes during this period. The magmatic lull from I-type hornblende biotite granodiorite (65.7 ± 0.7 Ma) to Paleocene A-type alkali feldspar granite (53.9 ± 0.3 Ma) probably reflects the transition from the latest Cretaceous compression to late Paleocene extension (Hwang et al., 2012; Myeong et al., 2018).

Magmatic activity has been considered absent between 60 and 48 Ma in Japan, which is most likely due to the small volume of igneous rocks (e.g., Iida et al., 2015). However, middle Paleocene–early Eocene igneous rocks have been reported in the southwestern area of the Inner Zone (the Sanin area), where they are described as part of the latest Cretaceous–Paleogene (68–52 Ma) igneous complexes (Takagi, 2004; Ishihara and Chappell, 2008; Jahn, 2010; Imaoka et al., 2011; Yakushiji et al., 2012; Ishihara and Tani, 2013; Nishida et al., 2013; Wakita, 2013; Koike and Tsutsumi, 2018, etc.). Unfortunately, the existing age determinations (mostly Rb–Sr) for rocks aged 60–52 Ma are not supported by geochemical composition data; thus, they cannot be compared and correlate with geochemical types of granitoids.

5. Subduction of the Izanagi-Pacific spreading ridge and contradictory data from the Shimanto belt geology

The idea of subduction of the spreading ridge separating the Kula (Izanagi) and Pacific oceanic plates has been used in the reconstructions of the Cretaceous–Paleogene geodynamic history of the Pacific margin of Asia for more than 40 years. However, the time of ridge subduction and related geological-tectonic events differ substantially in different publications (Uyeda and Miyashiro, 1974; Hilde et al., 1977; Maruyama and Send, 1986; Osozawa, 1992; Kiminami et al., 1994; Kinoshita, 1995; Nakajima, 1996; Maruyama et al., 1997; Whittaker et al., 2007; Isozaki et al., 2010; Raimbourg et al., 2014; Seton et al., 2015; Honda, 2016; Liu et al., 2017, 2020, etc.). Among these studies, the earliest age of ridge subduction is assumed to be the Late Cretaceous (90–80 Ma) (e.g., Uyeda and Miyashiro, 1974) while the youngest age is the middle Eocene (48–43 Ma) (e.g., Raimbourg et al., 2014).

Other researchers determined that the subduction time of the Izanagi-Pacific ridge was in the range of 60–55 Ma (e.g., Whittaker et al., 2007) or 60–50 Ma (e.g., Seton et al., 2015) and associated this process (e.g., spreading cessation in the Tasman Sea and change in the Australian plate drift direction from northwestern to northern) with the global Eocene reorganization of not only Pacific oceanic plates (e.g., the bend in the axis orientation of the Hawaiian Ridge-Emperor Seamount chain) but also Southern Indian Ocean plates (e.g., Seton et al., 2015). These authors drew such conclusions through the modeling of a set of oceanic paleo-age grids (linear magnetic anomalies)
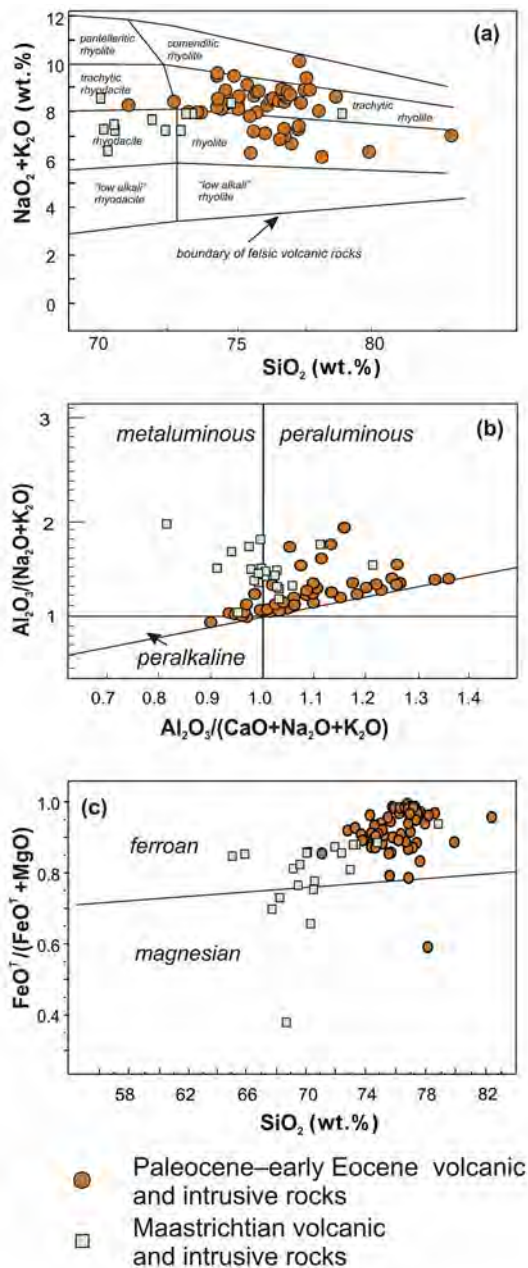
Fig. 5. Chemical classification and nomenclature diagrams for magmatic rocks from the Russian Far East. (a) Total alkalis-silica (TAS) diagram (after Le Bas et al., 1986); (b) A/NK ($Al_2O_3/(Na_2O + K_2O)$) vs. A/CNK ($Al_2O_3/(CaO + Na_2O + K_2O)$), all in molar quantities) diagram of Shand's index (Maniar and Piccoli, 1989); and (c) $FeO^T/(FeO^T + MgO)$ vs. SiO_2 diagram, including the boundary between ferroan and magnesian felsic rocks (in wt.%; Frost et al., 2001). Geochemical data from Popov and Grebennikov, 2001; Grebennikov and Maksimov, 2006, 2021; Alenicheva and Sakhno, 2008; Sakhno et al., 2010; Jahn et al., 2015; Petrov et al., 2015; Pavlyutkin et al., 2016; Tang et al., 2016; Zhao et al., 2017; and Sakhno and Kovalenko, 2018.

from 140 Ma to the present using the spreading symmetry principle and data on the preserved but multiple fragmented isochrons of magnetic anomalies within the modern northwestern Pacific. Other data, such as the positions of the modern mid-ocean ridges, their orientations with respect to the continental margins, and interpretations of the modern mantle structure beneath the eastern margin of Asia based on seismic tomography data, have also been considered. According to the abovementioned researchers, the subduction of the spreading ridge was accompanied by the opening of a slab window under the eastern

paleo-Asian margin along the length of the Japan trench and breakoff (separation) of the Izanagi Plate slab that caused the relative motion vector of the Pacific Plate to turn 44° counterclockwise (Engebretson, 1985), which in turn entailed the global motion direction reorganization of other conjugate oceanic plates.

Recently proposed versions of the Izanagi-Pacific ridge subduction are mainly based on the idea of a stratigraphic (age) gap during the formation of the Shimanto accretionary prism in the Paleocene, a structural unconformity in the early Cenozoic forearc basin sediments in the Paleocene–early Eocene, and a magmatic gap during the middle Paleocene–early Eocene (Kimura et al., 2019) or early–middle Eocene (Wu and Wu, 2019).

A geological record of the interaction between the continental and oceanic plates at 60–50 Ma is available for study in the Shimanto belt (Japan) (Fig. 8). In NE Japan, rocks that formed at the continent-ocean boundary in the specified time interval are not distinguished (are not exposed at the surface), while in Hokkaido and Sakhalin, they are intensely transformed as the result of collision of the island arc with the continental margin after 50 Ma (Zharov, 2004; Ueda, 2016).

The Shimanto belt of southwestern Japan is a classic example of an ancient accretionary prism that formed during the continuous Late Cretaceous–Miocene subduction of oceanic crust (Taira et al., 1988; Isozaki et al., 2010; Kimura et al., 2016, etc.). It consists of repeatedly alternating tectono-stratigraphic slices composed of coherent and melanged fragments of the sedimentary cover and the basaltic layer of the oceanic crust and separated by low-angle thrusts (e.g., Kimura et al., 2016, and references therein). Based on microfauna data (radiolaria and foraminifera), the Shimanto terrane is divided into Cretaceous and Cenozoic subterranes (Taira et al., 1988). A large thrust called the Nobeoka tectonic line on Kyushu Island, the Aki tectonic line on Shikoku Island, or the Gobo-Hagi tectonic line on the Kii Peninsula of Honshu Island is assumed to be the boundary between these terranes (e.g., Kimura et al., 2016). Traditional opinions based on early paleontological dating indicate that the youngest age for the Cretaceous part of the Shimanto belt is Maastrichtian and the oldest age for the Cenozoic part is the early Eocene, and these opinions are based on the occurrence of a stratigraphic (age) gap in the formation of this accretionary complex. Two alternative points of view have been proposed to explain this phenomenon. One group of researchers (e.g., Yamamoto et al., 2009; Isozaki et al., 2010, etc.) relates this gap to tectonic erosion that occurred during the subduction of topographically elevated objects on the oceanic plate (e.g., seamounts). The other group explains the gap by underplating the old part of an oceanic plate with a relatively younger one during the continuous subduction and dipping of the latter to a depth greater than is exposed by erosional processes at present (Ohmori et al., 1997; Kondo et al., 2005; Hamahashi et al., 2013, etc.). In current models (e.g., Kimura et al., 2019), this stratigraphic gap is associated with the Izanagi-Pacific ridge subduction, which has occurred nearly parallel to the trench. According to these authors' opinion, "the oceanic plate was buoyant as it was the thinnest dense plate, closest to the oceanic ridges. The encounter of the oceanic ridges with the trench, therefore, caused forearc uplift and a break in the development of accretionary prisms".

At the same time, a sufficient number of publications have indicated that a part of the structurally lowermost tectono-stratigraphic units of the Cretaceous Shimanto accretionary formations are aged to the Paleocene (Oyaizu et al., 2002; Oyaizu and Kiminami, 2004; Kitamura et al., 2005; Shibata et al., 2008; Bessho, 2015; Hara et al., 2017; Hara and Hara, 2019, etc.). For example, in the Kitagawa-Umaji area of Shikoku Island, the lowermost structural level of the Cretaceous part of the Shimanto accretionary complex, which forms the hanging wall of the Aki thrust, is represented by the Mugi tectono-stratigraphic complex (Kiminami et al., 1998; Hara et al., 2017, etc.). The upper part of the complex is composed of a melange (blocks and different-sized fragments of basalts, cherts, and sandstones in a foliated siltstone matrix), while the lower part consists of alternating phyllitic schists (originally
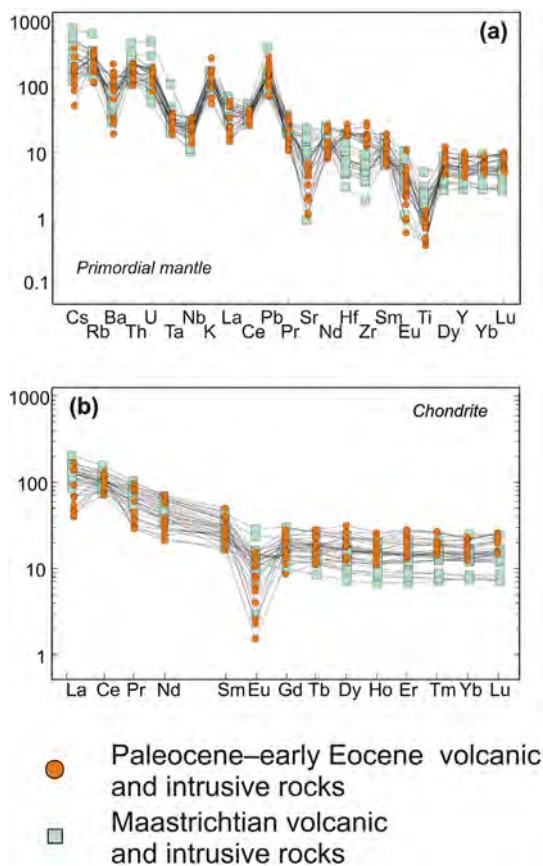
siltstones) and sandstones (see Fig. 8). Paleontological data indicate the Campanian–Maastrichtian age of the melange matrix (Ishida and Hashimoto, 1998; Kiminami et al., 1998; Hara et al., 2017). However, the results of U–Pb dating of detrital zircons show that the melange and coherent formations of the Mugi complex are of early Paleocene age. The youngest cluster of zircons from the melange matrix is 62.7 ± 1.7 Ma, and that from the sandstones of the lower part of the complex is 62.0 ± 1.3 Ma (Hara et al., 2017).

Similar age data for the Mugi complex were obtained on the eastern coast of Shikoku Island (Shibata et al., 2008), where it is represented by a set of sixfold repeated tectonic slices composed of foliated black siltstones and horizons of chaotic formations (melange containing blocks and fragments of siliceous mudstones, cherts, basalts, and sandstones) and interbeds of felsic tuffs. The results of U–Pb dating of zircons from the tuff interbeds indicate 66.2 ± 3.5 Ma to 76.2 ± 2.4 Ma for the upper slices and 57.9 ± 2.9 Ma to 63.5 ± 3.8 Ma for the lower slices. These data conform with the paleontological (radiolaria) determinations showing a Paleocene age of the lower structural units of the Mugi accretionary complex (Kitamura et al., 2005). Hence, the data provided above demonstrate the absence of any significant age gap in the terrigenous rocks of the Shimanto complex, although cross-sections of continuous latest Cretaceous–Paleocene sequences are rare due to the imbricate-thrust structure of the Shimanto belt.

On the other hand, the Paleocene–early Eocene deposits of the Shimanto belt are characterized by essentially terrigenous composition and an almost total absence of pelagic and hemipelagic sediments. For example, on the Kii Peninsula, the Paleocene sedimentary rocks of the Cenozoic part of the Shimanto belt (known as the Hikigawa belt) that compose the Otonashigawa complex are represented by alternating packages of sandstones and siltstones alternating with thick beds of coarse-grained sandstones and interbeds of conglomerates with a total thickness of ~2000 m (e.g., Nakaya, 2012; Bessho, 2015, etc.).

Thus, the formation of the Late Cretaceous accretionary prism in the Shimanto belt also continued into the early Paleocene. During the middle Paleocene–early Eocene, instead of accretionary prism formation, the accumulation of continental margin turbidites occurred.

6. Discussion

The absence of middle Paleocene to early Eocene (60.5–53 Ma) typical supra-subduction igneous rocks in the Sikhote-Alin and adjacent areas indicates that subduction along the eastern margin of the paleo-Asian continent ceased in the Paleocene. This conclusion is additionally confirmed by the absence of typical accretionary middle Paleocene–early Eocene prisms in the Shimanto belt (e.g., Kimura et al., 2019). In the case of continuous subduction, the cross-sections of these complexes should include fragments of the oceanic plate stratigraphic sequences. However, the sedimentary deposits of this time interval are represented by continental margin turbidites.

On the other hand, the wide occurrence of middle Paleocene to early Eocene volcanic-plutonic complexes prevents interpretation of the eastern margin of the paleo-Asian continent in the early Paleogene as a passive margin. Therefore, out of three alternative variants – passive margin, active subduction margin and active transform margin – only the last one remains possible.

The variations in the structural ensembles of different-aged tectonic-stratigraphic complexes of the Shimanto belt, i.e., the spatial orientations of the deformation structures in the melanged and coherent formations of which they are composed, provide additional evidence for this interpretation. In particular, the Mugi complex, which is the youngest (Maastrichtian) and structurally lowermost unit of the Cretaceous part of the Shimanto belt on Shikoku Island and forms the base of the hanging wall of the Aki thrust, consists of normal layered and melanged terrigenous rocks crumpled into asymmetric folds with different amplitudes and strikes of NE–E (50°–60°, in modern coordinates) (Ikesawa et al., 2005; Kitamura et al., 2005; Kimura et al., 2012, etc.). The analytical results of the abovementioned authors regarding the spatial geometry of the deformation elements in both cataclastic terrigenous rocks and melanges – Riedel shears (R), secondary Riedel shears or synthetic shears (P), Riedel antithetic shears (R'), T-fractures (T), Y-shears, and slickensides – show that rock deformation took place under the conditions of a simple thrust parallel to the deposit bedding and caused by low-angle oblique subduction.

Unlike the Mugi complex, within the Murotohanto complex (Murotohanto subbelt after Lewis and Byrne, 2001) or Naharigawa complex (Naharigawa Formation after Hara and Hara (2019)), which is the oldest (Paleocene–Eocene) and structurally uppermost tectonic-stratigraphic unit of the Cenozoic part of the Shimanto belt directly underlying the Aki thrust, two stages of deformation structures are distinguished. The first (early) stage, during which the sedimentary deposits were crumpled into asymmetric folds with different amplitudes and latitudinal (W–E) strikes (in modern coordinates), is manifested only in the northernmost part of the complex containing Paleocene microfauna (Lewis and Byrne, 2001). During the second (late) stage of deformation, the sedimentary deposits of the entire Murotohanto complex (both the northern and southern parts, the age of which is determined to be early to middle Eocene on the basis of microfauna) were crumpled into asymmetric folds with NE strikes. The difference in the orientations of the deformation elements in the rocks is approximately 30°, which indicates a counterclockwise rotation of the relative motion vector of an oceanic plate in the early Eocene and a change in the convergence angle (Lewis and Byrne, 2001).
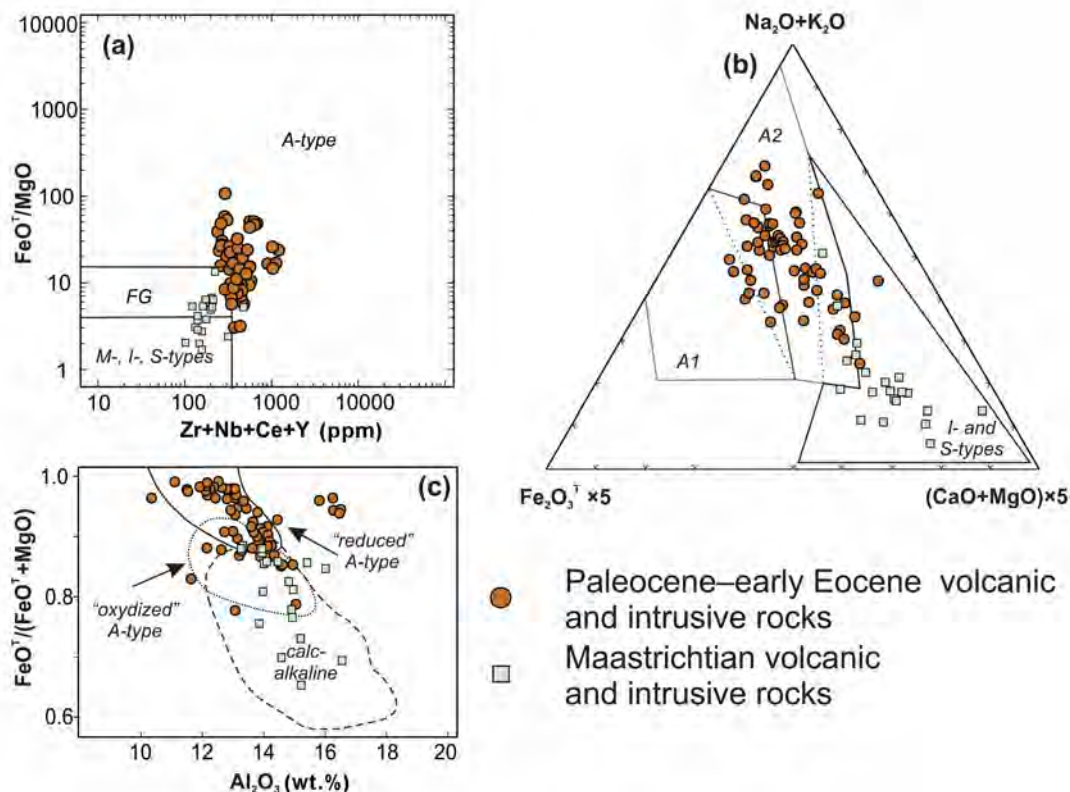
Fig. 7. Geochemical discrimination diagrams for magmatic rocks from the Russian Far East. (a) Zr + Nb + Ce + Y vs. FeO^T/MgO discrimination diagram for A-type granitoids; I-, S- and M-type and FG (highly fractionated granites) fields from Whalen et al., 1987; (b) variations in (Na$_2$O + K$_2$O) vs. Fe$_2$O$_3^T$ × 5 vs. (CaO + MgO) × 5 (in molar quantities; Grebennikov, 2014); and (c) FeO^T/(FeO^T + MgO) vs. Al$_2$O$_3$ diagram showing compositions of representative oxidized and reduced A-type granites compared with calc-alkaline granites (Dall'Agnol and De Oliveira, 2007). Geochemical data from Popov and Grebennikov, 2001; Grebennikov and Maksimov, 2006, 2021; Alenicheva and Sakhno, 2008; Sakhno et al., 2010; Jahn et al., 2015; Petrov et al., 2015; Pavlyutkin et al., 2016; Tang et al., 2016; Zhao et al., 2017; and Sakhno and Kovalenko, 2018.

Accounting for the difference between the kinematic regimes during formation of the deformation structures in the youngest unit of the Cretaceous Shimanto and the Paleocene and Eocene units of the Cenozoic Shimanto provides reasons to state that in the Late Cretaceous–early Eocene, the Pacific Plate changed its direction of motion twice with respect to the paleo-Asian margin, i.e., from the northwest (oblique subduction) in the Late Cretaceous to submeridional (middle to late Paleocene) and back to northwest (early Eocene). Note that the transform margin regime in the middle Paleocene–early Eocene (~60–53 Ma) is justified by the data from structural-biostratigraphic research on the Cenozoic part of the Shimanto belt (Hyuga complex) on Kyushu Island (Saito, 2008).

The change in the convergence angle of an oceanic plate is observed not only in the structural ensembles of accretionary complexes of the Shimanto belt but also in the formation of the structural complexes of back-arc formations. At this time, the eastern margin of the paleo-Asian continent was involved in intense strike-slip extension followed by the formation of significant large-scale W–NW linear volcanic depressions that transverse relative to the monolithic supra-subduction ESAVPB with a NE orientation. This, in turn, provides evidence that manifestations of volcanism occurred under the left-lateral activation of the N–NE fault system (e.g., Khanchuk, 2006; Utkin, 2013). Reports have postulated that tectonic inversion within the eastern paleo-Asian margin occurred in the Late Cretaceous–early Paleogene, thus reflecting the change from a compressional to an extensional setting. From 60 to 53 Ma, extension was widespread in Northeast China, Sikhote-Alin, Korea and adjacent areas along large-scale strike-slip faults (e.g., Ren

et al., 2002; Huang et al., 2015; Wang et al., 2018). This inversion is evidenced by the fault geometry and kinematics of the largest continental-scale strike-slip fault, the Tan-Lu fault system (TLFS) in Northeast China. After the gap in the Late Cretaceous, a new stage of sinistral motion along the TLFS in the early Paleogene was triggered by the NNW-directed movement of the Izanagi Plate along the Eurasian Plate from ~65–55 Ma (Wang et al., 2018).

Reports (Gladenkov et al., 2002; Ueda, 2016) have indicated that the closing of the Late Cretaceous forearc basin, which is currently situated within modern western Sakhalin and Hokkaido, started in the Paleocene as evidenced by the accumulation of Paleocene coarse clastic continental deposits with coal beds. In the South Sakhalin and Kamuikotan belts (Hokkaido), Late Cretaceous–early Paleocene accretionary complexes (~60 Ma) were crumpled into echelon systems of flexure-shaped folds followed by the exhumation of high-pressure metamorphic complexes in the middle Paleocene (Zharov, 2004; Ueda, 2016). The rapid exhumation of the accreted formations of the Paleo-Asian east margin continued also during Eocene time that evidenced by apatite double dating (U–Pb and fission track) and thermal history modeling of the granitoid massifs located within central and southern Sakhalin (Glorie et al., 2017).

This process is also evidenced by the fact that the Paleocene–early Eocene volcanic formations in the Sikhote-Alin overlie the clearly defined structural unconformity of the Late Cretaceous–early Paleocene supra-subduction magmatic complexes (e.g., Mikhailov, 1989). The youngest age of these complexes according to the U–Pb (SHRIMP) dating of diorites is 60.45 ± 0.65 Ma (Alenicheva and Sakhno, 2008), which
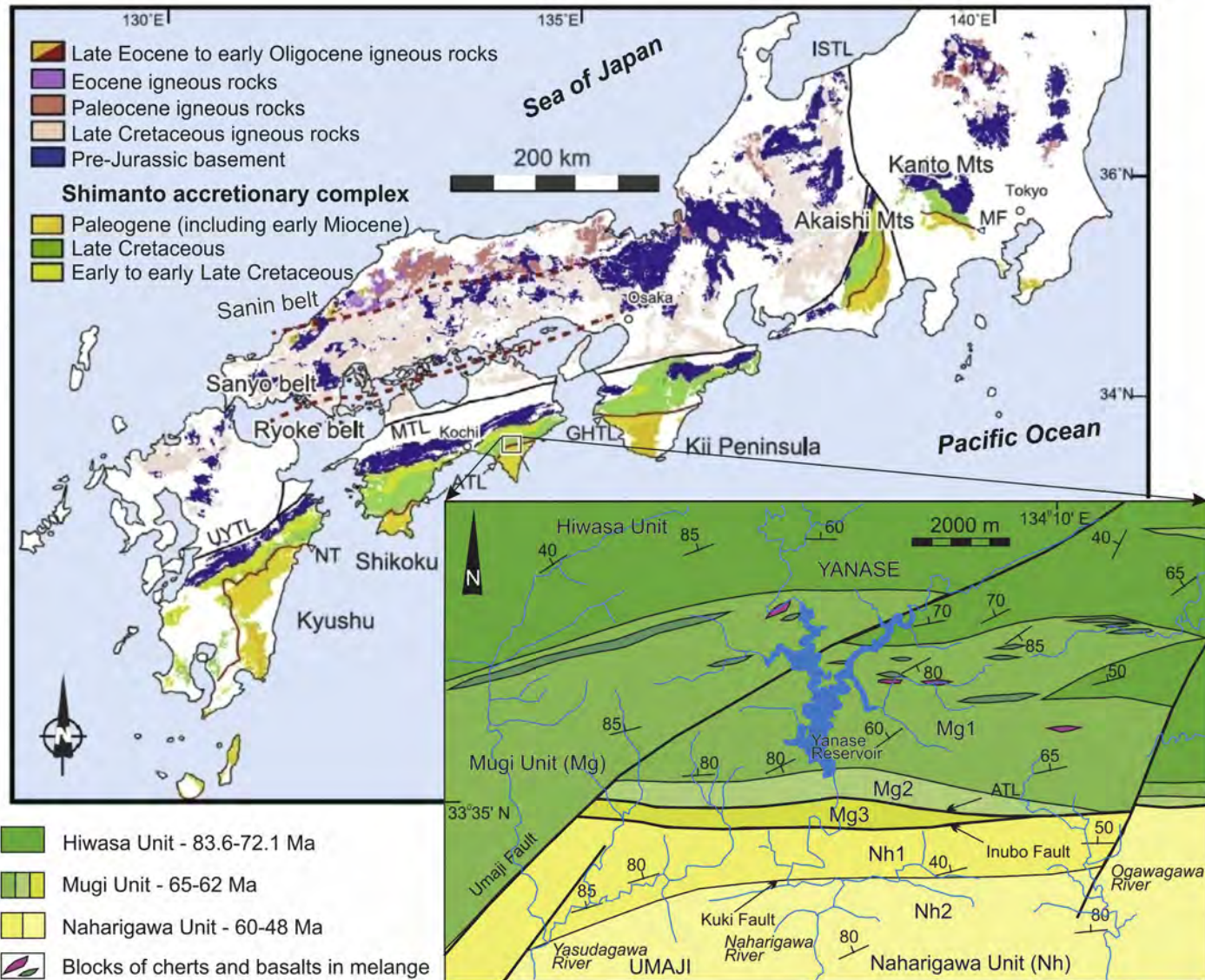
Fig. 8. Distribution and structure of the Shimanto accretionary belt (modified after Hara et al., 2017; Hara and Hara, 2019). The major tectonic lines in Southwest Japan are the Median Tectonic Line (MTL), Itoigawa–Shizuoka Tectonic Line (ISTL), and Usuki–Yatsushiro Tectonic Line (UYTL). The boundary between the Cretaceous and Paleogene Shimanto accretionary complexes is represented by the Nobeoka Thrust (NT) in Kyushu, Aki Tectonic Line (ATL) in Shikoku, Gobo–Hagi Tectonic Line (GHTL) in the Kii Peninsula, and the Matsuhime Fault (MF) in the Kanto Mountains.

is related to the age of the lowermost rhyolitic tuff (60.55 ± 0.10 Ma) of the verified middle Paleocene to early Eocene post-subduction magmatic activity in the Sikhote-Alin (Table 1).

Thus, starting from the middle Paleocene (~60.5 Ma), the geodynamic regime at the eastern margin of the paleo-Asian continent altered due to a change in the vector of relative motion of the Paleo-Pacific Plate from N–W to almost submeridional (Engebretson, 1985; Seton et al., 2015; Kononov and Lobkovsky, 2019, etc.). This change in the geodynamic mode in East Asia is usually described as a result of the subparallel Izanagi-Pacific ridge crest–trench intersection (e.g., Whittaker et al., 2007; Seton et al., 2015). However, magmatic manifestations of a slab window have not been established either in the Shimanto belt or in the synchronous forearc basin sediments (Raimbourg et al., 2014; Kimura et al., 2019), which contradicts the intersection of the continental margin with an active spreading ridge. Additionally, the continental rim of the northwest Pacific is marked by exotic Late Cretaceous–Paleocene island arc rocks that extend from Hokkaido, Japan, and southern Sakhalin across Kamchatka to the Koryak Highlands of Russia (e.g., Nokleberg et al., 2000; Konstantinovskaia, 2001; Zharov, 2004; Alexeiev et al., 2006; Ueda, 2016; Domeier et al., 2017; Vaes et al., 2019). The accretion history of these rocks cannot be explained by conventional tectonic models of the Pacific in which subduction is restricted to the eastern continental margin of Asia (Seton et al., 2012, 2015; Müller et al., 2016); however, the models do not take into account the existence of volcanic arcs between the continent and the Pacific Plate in the Late Cretaceous–Paleocene (Domeier et al., 2017). In the Hidaka zone of central Hokkaido, the described magmatic rocks related to ridge-trench-island arc collision are at dated to 55 Ma (Maeda and Kagami, 1996).

The magmatic gap thought to be observed in East Asia at 56–46 Ma (Wu and Wu, 2019) occurred between 53 and 46 Ma according to our data in the Sikhote-Alin, and in southwestern Japan, this gap is identified between 52 and 43 Ma (Imaoka et al., 2011). Moreover, the assumed relation of this gap to the subduction of an active spreading ridge (Wu and Wu, 2019) is inconsistent with the known data on the required occurrence of igneous rocks as a result of such interaction (e.g., Lagabrielle et al., 2000; Weigand et al., 2002).

A model showing that the Izanagi-Pacific ridge ceased activity along a continental margin (or trench) and thus stalled subduction and a transform margin was created parallel to the continental margin, followed by the breakoff of the lower (larger) part of the slab provides a possible explanation for the post-subduction magmatism in East Asia at 60–53 Ma. The geochemical diversity of tholeiitic (subalkaline) or even calc-alkaline (in Japan), adakitic (in NE China), and A-type rocks (in South Korea and Sikhote-Alin) that formed above the slab tear was mainly caused by the interaction between the upwelling anhydrous subslab mantle and the slab, while magma ascended along pathways through the subcontinental lithospheric mantle and the overlying crust. Injected through a slab tear, the subslab asthenosphere provided a mantle source for post-subduction magmas.

Coexistence of the mentioned above igneous magmatic series association has been widely reported in regions that formed above the slab tear, such as Late Miocene to Quaternary rocks of Baja California, Mexico (e.g., Benoit et al., 2002; Pallares et al., 2007). The geochemical diversity of transform margin igneous rocks is determined by their location relative to the former forearc and back-arc regions. The formation of acidic melts of the geochemical A-type has not been clarified (see review Bonin, 2007; Dall'Agnol et al., 2012). However, most researchers have concluded that they indicate intracontinental extension caused by a change of a geodynamic mode (from transpression to transtension) and could not have occurred in the orthogonal or oblique subduction setting that leads to compressional conditions at a convergent margin (Bonin et al., 1998; Grebennikov et al., 2016; Robinson et al., 2017, etc.). In the case of ridge subduction, petro-geochemical types of igneous rocks that present coexisting tholeiitic, calc-alkaline or adacitic intermediate and felsic compositions formed due to the heating and
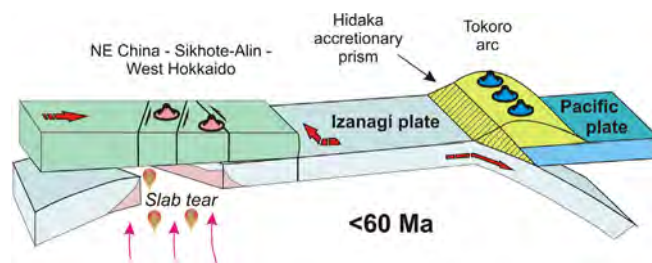
Fig. 9. Geodynamic model of slab tear formation in the East Asia continental margin due to a change in the direction of the oceanic plate movement at the middle Paleocene.

partial melting of the accretionary prism rocks ('blowtorch' effect); an example includes Pliocene–Quaternary igneous rocks of the Chile Triple Junction (Lagabrielle et al., 2000) or latest Oligocene to Middle Miocene ridge-crest–trench intersection post-subduction volcanism in western and offshore California (Cole and Basu, 1995; Weigand et al., 2002). When the geodynamic mode of subduction of an oceanic plate changes to transform sliding, a slab tear forms some distance from the ocean-continent boundary in the stalled slab, which is illustrated by the Baja California example (Pallares et al., 2007; Castillo, 2008). Middle Paleocene–early Eocene post-subduction magmatic rocks of East Asia have been found only far away behind the Paleocene continent-ocean boundary. These data are consistent with the slab tearing model but contradict the Izanagi-Pacific ridge subduction model. We do not deny that Izanagi-Pacific ridge subduction occurred; however, the presented data indicate its absence beneath the East Asia continental margin (Sea of Japan region) in the considered time interval. These data are consistent with the model of final subduction of the Izanagi plate beneath the island arc in the North Pacific (Domeier et al., 2017).

Note that after 53 Ma, a dramatic change in strike-slip displacements from sinistral to dextral occurred in the TLFS (Huang et al., 2015; Wang et al., 2018), which coincided with the collision of the Late Cretaceous–early Eocene island arc system of eastern Hokkaido and Sakhalin with the continent from 45 to 38 Ma (Zharov, 2004; Jahn et al., 2014; Ueda, 2016; Alexandrov et al., 2018; Liao et al., 2018; Zhao et al., 2018). Starting from the early Eocene, fault-related coal-bearing depressions began to form within the Sikhote-Alin area (Pavlyutkin et al., 2016) in a setting of NE compression in paragenetic connection with N- and N–NE-striking dextral strike-slip faults and NE- and E–NE-striking normal faults (Golozubov et al., 2007, 2009). Calc-alkaline basalts separate the lower coal-bearing strata from the upper ones, and their different lithological compositions and floral complexes provide a type of benchmark. K–Ar dating indicates that these rocks correspond to the middle Eocene 45.7–45.1 Ma (Pavlyutkin et al., 2016). The earliest volcanic eruptions of adakites in the southwest zone of the Sikhote-Alin area have similar K–Ar age data from 45.5 ± 1.1 Ma to 46.2 ± 0.5 Ma (Chashchin et al., 2011, and references therein) and geochemical features analogous to those of high-Mg adakitic rocks (44–38 Ma) from the Kitakami Mountains, Japan (Tsuchiya et al., 2005).

Thus, the middle Paleocene–early Eocene magmatism of East Asia related to a transform margin can be described by a model of slab tear formation in the continental margin due to a change in the direction of the oceanic plate movement possibly connected to the Izanagi-Pacific ridge death along the continental margin or its collision with an island arc (Fig. 9).

7. Conclusions

Original and published isotopic and geochemical data have been analyzed to determine the age limit of the post-subduction strike-slip igneous activity in the Sikhote-Alin (southeastern Russia) region and to justify a middle Paleocene to early Eocene magmatic stage from 60.5–53 Ma. These middle Paleocene–early Eocene igneous rocks,

including calc-alkaline, adakitic, and A-type granites and related volcanic rocks, are also distributed elsewhere in East Asia, such as Northeast China, the southern Korean Peninsula, and the Inner Zone of Japan.

The interval of post-subduction magmatic activity in East Asia (60.5–53 Ma) coincides with the new (after the Turonian–early Paleocene time interval) stage of sinistral displacements along the Tan-Lu fault system but is not consistent with the formation period of the subduction-related Cenozoic accretionary prism of the Shimanto belt, which confirms the idea of a middle Paleocene–early Eocene transform continental margin along the northern part of East Asia.

The absence in the Shimanto belt of igneous rocks related to the slab window caused by subduction of the spreading ridge can be explained by a model in which the Izanagi-Pacific ridge ceases along a continental margin or collided with an island arc, thereby stalling subduction and resulting in the formation of a transform margin accompanied by the upwelling of subslab asthenosphere through a slab tear, which is analogous to the findings for Baja California. According to this model, slab tears form some distance from the ocean-continent boundary and post-subduction magmatic complexes (60.5–53 Ma) consisting mostly of A-type rocks naturally form in extension regions of the East Asian continent.

Declaration of competing interest

Acknowledgements

References

Alenicheva, A.A., Sakhno, V.G., 2008. The U-Pb dating of extrusive-intrusive complexes in ore districts in the Southern part of the Eastern Sikhote-Alin volcanic belt (Russia). Dokl. Earth Sci. 419, 217–221.

Alexandrov, I.A., Liao, J.P., Jahn, B.M., Golozoubov, V.V., Ivin, V.V., Stepnova, Y.A., 2018. Eocene granitoids of the Okhotsk granodiorite complex (South Sakhalin). Dokl. Earth Sci. 483, 1499–1503.

Alexeiev, D.V., Gaedicke, C., Tsukanov, N.V., Freitag, R., 2006. Collision of the Kronotskiy arc at the NE Eurasia margin and structural evolution of the Kamchatka–Aleutian junction. Int. J. Earth Sci. 95, 977–993.

Benoit, M., Aguillón-Robles, A., Calmus, T., Maury, R.C., Bellon, H., Cotten, J., Bourgois, J., Michaud, F., 2002. Geochemical diversity of late miocene volcanism in Southern Baja California, Mexico: implication of mantle and crustal sources during the opening of an asthenospheric window. J. Geol. 110, 627–648.

Bessho, T., 2015. How are the roofing and unroofing processes reflected in sandstone composition? A case study in the Shimanto Belt, Kii Peninsula, Southwestern Japan. J. Sedimentol. Soc. Jpn. 74, 3–20.

Bonin, B., 2007. A-type granites and related rocks: evolution of a concept, problems and prospects. Lithos 97, 1–29.

Bonin, B., Azzouni-Sekkal, A., Bussy, F., Ferrag, S., 1998. Alkali-calcic and alkaline post-orogenic (PO) granite magmatism: petrologic constraints and geodynamic settings. Lithos 45, 45–70.

Castillo, P.R., 2008. Origin of the adakite-high-Nb basalt association and its implications for postsubduction magmatism in Baja California. Mexico. Geol. Soc. Am. Bull. 120, 451–462.

Chashchin, A.A., Nechaev, V.P., Nechaeva, E.V., Blokhin, M.G., 2011. Discovery of Eocene adakites in Primor'e. Dokl. Earth Sci. 438, 744–749.

Cheong, C.S., Yi, K., Kim, N., Lee, T.H., Lee, S.R., Geng, J.Z., Li, H.K., 2013. Tracking source materials of Phanerozoic granitoids in South Korea by zircon Hf isotopes. Terra Nova 25, 228–235.

Cole, R.B., Basu, A.R., 1995. Nd-Sr isotopic geochemistry and tectonics of ridge subduction and middle Cenozoic volcanism in Western California. Geol. Soc. Am. Bull. 107, 167–179.

Dall'Agnol, R., De Oliveira, D.C., 2007. Oxidized, magnetite-series, rapakivi-type granites of Carajás, Brazil: implications for classification and petrogenesis of A-type granites. Lithos 93, 215–233.

Dall'Agnol, R., Frost, C.D., Rämö, O.T., 2012. IGCP project 510 "A-type granites and related rocks through time": project vita, results, and contribution to granite research. Lithos 151, 1–16.

Domeier, M., Shephard, G.E., Jakob, J., Gaina, C., Doubrovine, P.V., Torsvik, T.H., 2017. Intraoceanic subduction spanned the Pacific in the late Cretaceous–Paleocene. Sci. Adv. 3, eaao2303.

Engebretson, D.C., 1985. Relative motions between oceanic and continental plates in the Pacific basin. Geol. Soc. Am. Spec. Pap. 206, 1–59.

Frost, B.R., Barnes, C.G., Collins, W.J., Arculus, R.J., Ellis, D.J., Frost, C.D., 2001. A geochemical classification for granitic rocks. J. Petrol. 42, 2033–2048.

Gladenkov, Y.B., Bazhenova, O.K., Grechin, V.I., Margulis, L.S., Sal'nikov, B.A., 2002. Cenozoic History and Oil-and-Gas-Bearing Potential of Sakhalin. GEOS, Moscow.

Glorie, S., Alexandrov, I., Nixon, A., Jepson, G., Gillespie, J., Jahn, B.-M., 2017. Thermal and exhumation history of Sakhalin Island (Russia) constrained by apatite U-Pb and fission track thermochronology. J. Asian Earth Sci. 143, 326–342.

Golozubov, V., Miklovda, S., Lee, D.-W., Pavlyutkin, B., Kasatkin, S., 2007. Dynamics of the formation of the Cenozoic Uglovsky basin (Southern Primorye). Russ. J. Pac. Geol. 1, 324–334.

Golozubov, V., Li, D.U., Kasatkin, S., Pavlyutkin, B., 2009. Tectonics of the Cenozoic Nizhnii Bikin coaliferous depression in the Northern Primorye region. Russ. J. Pac. Geol. 3, 269–283.

Golozubov, V.V., Khanchuk, A.I., 1995. Taukha and Zhuravlevka Terranes South Sikhote-Alin: a fragments of early cretaceous Asia continental margin. Russ. J. Pac. Geol. 14, 13–26.

Grebennikov, A.V., 2011. Silica-metal spherules in ignimbrites of Southern Primorye. Russ. J. Earth Sci. 22, 20–31.

Grebennikov, A.V., 2014. A-type granites and related rocks: petrogenesis and classification. Russ. Geol. Geophys. 55, 1353–1366.

Grebennikov, A.V., Maksimov, S.O., 2006. Fayalite rhyolites and a zoned magma chamber of the Paleocene Yakutinskaya volcanic depression in Primorye. Russia. J. Mineral. Petrol. Sci. 101, 69–88.

Grebennikov, A.V., Maksimov, S.O., 2021. Reasons for the occurrence of A-type volcanic rocks at the active continental margins (South Sikhote-Alin, Russian Far East). Russ. Geol. Geophys. 62 (2). https://doi.org/10.15372/RGG2020114.

Grebennikov, A.V., Popov, V.K., 2014. Petrogeochemical aspects of the late cretaceous and Paleogene ignimbrite volcanism of East Sikhote-Alin. Russ. J. Pac. Geol. 8, 38–55.

Grebennikov, A.V., Shcheka, S.A., Karabtsov, A.A., 2012. Silicate-metallic spherules and the problem of the ignimbrite eruption mechanism: the Yakutinskaya volcanic depression. J. Volcanol. Seismol. 6, 211–229.

Grebennikov, A.V., Khanchuk, A.I., Gonevchuk, V.G., Kovalenko, S.V., 2016. Cretaceous and Paleogene granitoid suites of the Sikhote-Alin area (Far East Russia): geochemistry and tectonic implications. Lithos 261, 250–261.

Grebennikov, A.V., Kasatkin, S.A., Fedoseev, D.G., Khanchuk, A.I., 2020. The Middle Paleocene–Early Eocene (60.5–53.0 Ma) magmatic stage in the Southern Russian Far East. Russ. J. Pac. Geol. 14, 415–420.

Guo, F., Nakamuru, E., Fan, W., Kobayoshi, K., Li, C., 2007. Generation of Palaeocene adakitic andesites by magma mixing; Yanji Area, NE China. J. Petrol. 48, 661–692.

Hamahashi, M., Saito, S., Kimura, G., Yamaguchi, A., Fukuchi, R., Kameda, J., Hamada, Y., Kitamura, Y., Fujimoto, K., Hashimoto, Y., 2013. Contrasts in physical properties between the hanging wall and footwall of an exhumed seismogenic megasplay fault in a subduction zone—an example from the Nobeoka thrust drilling project. Geochem. Geophys. Geosyst. 14, 5354–5370.

Hara, H., Hara, K., 2019. Radiolarian and U–Pb zircon dating of late cretaceous and Paleogene Shimanto accretionary complexes, Southwest Japan: temporal variations in provenance and offset across an out-of-sequence thrust. J. Asian Earth Sci. 170, 29–44.

Hara, H., Nakamura, Y., Hara, K., Kurihara, T., Mori, H., Iwano, H., Danhara, T., Sakata, S., Hirata, T., 2017. Detrital zircon multi-chronology, provenance, and low-grade metamorphism of the C retaceous S himanto accretionary complex, Eastern Shikoku, Southwest Japan: tectonic evolution in response to igneous activity within a subduction zone. Isl. Arc 26, e12218.

Hilde, T.W.C., Uyeda, S., Kroenke, L., 1977. Evolution of the Western Pacific and its margin. Tectonophys. 38, 145–165.

Honda, S., 2016. Slab stagnation and detachment under Northeast China. Tectonophys. 671, 127–138.

Huang, L., Liu, C.Y., Kusky, T.M., 2015. Cenozoic evolution of the Tan–Lu Fault Zone (East China)—Constraints from seismic data. Gondwana Res. 28, 1079–1095.

Hwang, B.H., Ernst, W.G., Yang, K., 2012. Two different magma series imply a Palaeogene tectonic transition from contraction to extension in the SE Korean Peninsula. Int. Geol. Rev. 54, 1284–1295.

Ichikawa, K., Mizutani, S., Hara, I., Hada, S., Yao, A., 1990. Pre-cretaceous Terranes of Japan. Publication of IGCP Project No. 224. Pre-Jurassic Evolution of Eastern Asia, Nihon-Insatsu, Osaka.

Iida, K., Iwamori, H., Orihashi, Y., Park, T., Jwa, Y.J., Kwon, S.T., Danhara, T., Iwano, H., 2015. Tectonic reconstruction of batholith formation based on the spatiotemporal distribution of C retaceous–P aleogene granitic rocks in Southwestern Japan. Isl. Arc 24, 205–220.

Ikeda, T., Harada, T., Kouchi, Y., Morita, S., Yokogawa, M., Yamamoto, K., Otoh, S., 2016. Provenance analysis based on detritalzirconage spectra of the lower cretaceous formations in the Ryoseki-Monobe Area, outer zone of Southwest Japan. Mem. Fukui Prefect. Dinosaur Mus. 15, 33–84.

Ikesawa, E., Kimura, G., Sato, K., Ikehara-Ohmori, K., Kitamura, Y., Yamaguchi, A., Ujiie, K., Hashimoto, Y., 2005. Tectonic incorporation of the upper part of oceanic crust to overriding plate of a convergent margin: an example from the Cretaceous–early Tertiary Mugi Mélange, the Shimanto Belt. Japan. Tectonophys. 401, 217–230.

Imaoka, T., Kiminami, K., Nishida, K., Takemoto, M., Ikawa, T., Itaya, T., Kagami, H., Iizumi, S., 2011. K–Ar age and geochemistry of the SW Japan Paleogene cauldron cluster: implications for Eocene–Oligocene thermo-tectonic reactivation. J. Asian Earth Sci. 40, 509–533.

Ishida, K., Hashimoto, H., 1998. Upper cretaceous radiolarian biostratigraphy in selected chert-clastic sequences of the North Shimanto Terrane. East Shikoku. News Osaka Micropaleontol. 11, 211–225.

Ishihara, S., Chappell, B.W., 2008. Chemical compositions of the Paleogene granitoids of Eastern Shimane prefecture, Sanin district, Southwest Japan. Bull. Geol. Surv. Jpn 59, 225–254.

Ishihara, S., Tani, K., 2013. Zircon age of granitoids hosting molybdenite-quartz vein deposits in the central Sanin Belt. Southwest Japan. Shigen-Chishitsu (Resour. Geol.) 63, 11–14.

Isozaki, Y., Aoki, K., Nakama, T., Yanai, S., 2010. New insight into a subduction-related orogen: a reappraisal of the geotectonic framework and evolution of the Japanese Islands. Gondwana Res. 18, 82–105.

Jahn, B.M., 2010. Accretionary orogen and evolution of the Japanese Islands: implications from a Sr-Nd isotopic study of the Phanerozoic granitoids from SW Japan. Am. J. Sci. 310, 1210–1249.

Jahn, B.M., Usuki, M., Usuki, T., Chung, S.L., 2014. Generation of Cenozoic granitoids in Hokkaido (Japan): constraints from zircon geochronology, Sr-Nd-Hf isotopic and geochemical analyses, and implications for crustal growth. Am. J. Sci. 314, 704–750.

Jahn, B.M., Valui, G., Kruk, N., Gonevchuk, V., Usuki, M., Wu, J.T.J., 2015. Emplacement ages, geochemical and Sr–Nd–Hf isotopic characterization of Mesozoic to early Cenozoic granitoids of the Sikhote-Alin Orogenic Belt. Russian Far East: crustal growth and regional tectonic evolution. J. Asian Earth Sci. 111, 872–918.

Kemkin, I., 2008. Structure of terranes in a Jurassic accretionary prism in the Sikhote-Alin-Amur area: implications for the Jurassic geodynamic history of the Asian Eastern margin. Russ. Geol. Geophys. 49, 759–770.

Kemkin, I., Khanchuk, A.I., Kemkina, R., 2016. Accretionary prisms of the Sikhote-Alin Orogenic belt: composition, structure and significance for reconstruction of the geodynamic evolution of the Eastern Asian margin. J. Geodyn. 102, 202–230.

Kemkin, I.V., 2006. Geodynamic Evolution of the Sikhote-Alin and Japan Sea Region in Mesozoic. Nauka, Moscow.

Khanchuk, A.I., 2001. Pre-Neogene tectonics of the Sea-of-Japan region: a view from the Russian side. Earth Sci. (Chikyu Kagaku) 55, 275–291.

Khanchuk, A.I., 2006. Geodynamics, Magmatism and Metallogeny of the Russian East. Dal'nauka, Vladivostok.

Khanchuk, A.I., Kemkin, I.V., Kruk, N.N., 2016. The Sikhote-Alin orogenic belt, Russian South East: terranes and the formation of continental lithosphere based on geological and isotopic data. J. Asian Earth Sci. 120, 117–138.

Khanchuk, A.I., Grebennikov, A.V., Ivanov, V.V., 2019. Albian–Cenomanian orogenic belt and igneous province of Pacific Asia. Russ. J. Pac. Geol. 13, 187–219.

Kiminami, K., Miyashita, S., Kawabata, K., 1994. Ridge collision and in situ greenstones in accretionary complexes: an example from the late cretaceous Ryukyu Islands and Southwest Japan margin. Isl. Arc 3, 103–111.

Kiminami, K., Matsuura, T., Iwata, T., Miura, K., 1998. Relationship between sandstone composition in the cretaceous Shimanto supergroup, Eastern Shikoku, and cretaceous arc volcanism. J. Geol. Soc. Jpn. 104, 314–326.

Kimura, G., Yamaguchi, A., Hojo, M., Kitamura, Y., Kameda, J., Ujiie, K., Hamada, Y., Hamahashi, M., Hina, S., 2012. Tectonic mélange as fault rock of subduction plate boundary. Tectonophys. 568, 25–38.

Kimura, G., Hashimoto, Y., Yamaguchi, A., Kitamura, Y., Ujiie, K., 2016. Cretaceous–Neogene accretionary units: Shimanto belt. In: Moreno, T., Wallis, S., Kojima, T., Gibbons, W. (Eds.), The Geology of Japan. The Geological Society, London, pp. 125–137.

Kimura, G., Kitamura, Y., Yamaguchi, A., Kameda, J., Hashimoto, Y., Hamahashi, M., 2019. Origin of the early Cenozoic belt boundary thrust and Izanagi–Pacific ridge subduction in the Western Pacific margin. Isl. Arc 28, e12320.

Kinoshita, O., 1995. Migration of igneous activities related to ridge subduction in Southwest Japan and the East Asian continental margin from the Mesozoic to the Paleogene. Tectonophys. 245, 25–35.

Kitamura, Y., Sato, K., Ikesawa, E., Ikehara-Ohmori, K., Kimura, G., Kondo, H., Ujiie, K., Onishi, C.T., Kawabata, K., Hashimoto, Y., 2005. Mélange and its seismogenic roof décollement: a plate boundary fault rock in the subduction zone—an example from the Shimanto Belt, Japan. Tectonics 24, TC5012.

Koike, W., Tsutsumi, Y., 2018. Zircon U-Pb dating of plutonic rocks at the Tsukuba area. Central Japan. Bull. Natl. Mus. Nat. Sci. Ser. C 1–11.

Kojima, S., 1989. Mesozoic terrane accretion in Northeast China, Sikhote-Alin and Japan regions. Palaeogeogr. Palaeoclimatol. Palaeoecol. 69, 213–232.

Kondo, H., Kimura, G., Masago, H., Ohmori-Ikehara, K., Kitamura, Y., Ikesawa, E., Sakaguchi, A., Yamaguchi, A., Okamoto, S.Y., 2005. Deformation and fluid flow of a major out-of-sequence thrust located at seismogenic depth in an accretionary complex: Nobeoka Thrust in the Shimanto Belt, Kyushu, Japan. Tectonics 24, TC6008.

Kononov, M.V., Lobkovsky, L.I., 2019. Influence of the upper mantle convection cell and related Pacific plate subduction on Arctic Tectonics in the late Cretaceous–Cenozoic. Geotectonics 53, 658–674.

Konstantinovskaia, E.A., 2001. Arc–continent collision and subduction reversal in the Cenozoic evolution of the Northwest Pacific: an example from Kamchatka (NE Russia). Tectonophys. 333, 75–94.

Lagabrielle, Y., Guivel, C., Maury, R.C., Bourgois, J., Fourcade, S., Martin, H., 2000. Magmatic–tectonic effects of high thermal regime at the site of active ridge subduction: the Chile Triple Junction model. Tectonophys. 326, 255–268.

Le Bas, M.J., Le Maitre, R.W., Streckeisen, A., Zanettin, B., IUGS Subcommission on the Systematics of Igneous Rocks, 1986. A chemical classification of volcanic rocks based on the total alkali-silica diagram. J. Petrol. 27, 745–750.

Lewis, J.C., Byrne, T.B., 2001. Fault kinematics and past plate motions at a convergent plate boundary: tertiary Shimanto belt, Southwest Japan. Tectonics 20, 548–565.

Li, P.C., Liu, Z.H., Li, S.C., Zhao, Q.Y., Shi, Q., Li, C.H., Yang, X.H., 2018. Late Paleocene–early Eocene granitoids in the Jiamusi Massif, NE China: Zircon U–Pb ages, geochemistry, and tectonic implications. Int. Geol. Rev. 61, 1–16.

Liao, J.P., Jahn, B.M., Alexandrov, I., Chung, S.L., Zhao, P., Ivin, V., Usuki, T., 2018. Petrogenesis of Mid-Eocene granites in South Sakhalin, Russian Far East: Juvenile crustal growth and comparison with granitic magmatism in Hokkaido and Sikhote-Alin. J. Asian Earth Sci. 167, 103–129.

Liu, K., Zhang, J., Xiao, W., Wilde, S.A., Alexandrov, I., 2020. A review of magmatism and deformation history along the NE Asian margin from ca. 95 to 30 Ma: transition from the Izanagi to Pacific plate subduction in the early Cenozoic. Earth-Sci. Rev. 209, 103317.

Liu, X., Zhao, D., Li, S., Wei, W., 2017. Age of the subducting Pacific slab beneath East Asia and its geodynamic implications. Earth Planet. Sci. Lett. 464, 166–174.

Maeda, J.i., Kagami, H., 1996. Interaction of a spreading ridge and an accretionary prism: implications from MORB magmatism in the Hidaka magmatic zone, Hokkaido, Japan. Geology 24, 31–34.

Malinovsky, A.I., 2019. Source areas and geodynamic settings of Cenozoic deposits in the West Sakhalin terrane based on the results of study of heavy detrial minerals. Bull. Kamchatka Reg. Assoc. Educ. Sci. Cent. Earth Sci. 3, 5–25.

Maniar, P.D., Piccoli, P.M., 1989. Tectonic discrimination of granitoids. Geol. Soc. Am. Bull. 101, 635–643.

Martynov, Y.A., Khanchuk, A.I., Grebennikov, A.V., Chashchin, A.A., Popov, V.K., 2017. Late Mesozoic and Cenozoic volcanism of the East Sikhote-Alin area (Russian Far East): a new synthesis of geological and petrological data. Gondwana Res. 47, 358–371.

Maruyama, S., Send, T., 1986. Orogeny and relative plate motions: example of the Japanese Islands. Tectonophys. 127, 305–329.

Maruyama, S., Isozaki, Y., Kimura, G., Terabayashi, M., 1997. Paleogeographic maps of the Japanese Islands: plate tectonic synthesis from 750 Ma to the present. Isl. Arc 6, 121–142.

McDonough, W.F., Sun, S.S., 1995. The composition of the Earth. Chem. Geol. 120, 223–253.

Mikhailov, V.A., 1989. The Magmatism of Volcanotectonic Structures in the Southern Segments of the East Sikhote-Alin Volcanic Belt. Far East Branch Russian Academy of Science, Vladivostok.

Mizutani, S., Kojima, S., 1992. Mesozoic radiolarian biostratigraphy of Japan and collage tectonics along the Eastern continental margin of Asia. Palaeogeogr. Palaeoclimatol. Palaeoecol. 96, 3–22.

Moreno, T., Wallis, S., Kojima, T., Gibbons, W., 2016. The Geology of Japan. Geol. Soc, London.

Müller, R.D., Seton, M., Zahirovic, S., Williams, S.E., Matthews, K.J., Wright, N.M., Shephard, G.E., Maloney, K.T., Barnett-Moore, N., Hosseinpour, M., 2016. Ocean basin evolution and global-scale plate reorganization events since Pangea breakup. Annu. Rev. Earth Planet. Sci. 44, 107–138.

Myeong, B., Kim, J.H., Woo, H.D., Jang, Y.D., 2018. Origin of the Eocene Gyeongju A-type granite, SE Korea: implication for the high fluorine contents. Econ. Environ. Geol. 51, 439–453.

Nakajima, T., 1996. Cretaceous granitoids in SW Japan and their bearing on the crust-forming process in the Eastern Eurasian margin. Geol. Soc. Am. Spec. Pap. 315, 183–191.

Nakaya, S., 2012. Reconsideration of the "Nyunokawa Formation" of the Shimanto Belt in the Kii Peninsula, Southwest Japan. Assoc. Geol. Collab. Jpn. Monogr. 59, 51–60.

Nishida, K., Imaoka, T., Kiminami, K., Nagamatsu, Y., Iizumi, S., 2013. Marked change of Sr–Nd isotopic compositions of granitoids in Sanin Belt of SW Japan and Gyeongsang Basin of Korea during the latest cretaceous, and geologic significance. J. Geol. Soc. Jpn. 119, 229–248.

Nokleberg, W.J., Parfenov, L.M., Monger, J.W.H., Norton, I.O., Khanchuk, A.I., Stone, D.B., Scotese, C.R., Scholl, D.W., Fujita, K., 2000. Phanerozoic Tectonic Evolution of the Circum-North Pacific. USGS Professional Paper 1626. California, CA, USGS.

Ohmori, K., Taira, A., Tokuyama, H., Sakaguchi, A., Okamura, M., Aihara, A., 1997. Paleothermal structure of the Shimanto accretionary prism, Shikoku, Japan: role of an out-of-sequence thrust. Geology 25, 327–330.

Osozawa, S., 1992. Double ridge subduction recorded in the Shimanto accretionary complex, Japan, and plate reconstruction. Geology 20, 939–942.

Otofuji, Y.I., Matsuda, T., 1983. Paleomagnetic evidence for the clockwise rotation of Southwest Japan. Earth Planet. Sci. Lett. 62, 349–359.

Otofuji, Y.I., Matsuda, T., 1987. Amount of clockwise rotation of Southwest Japan—fan shape opening of the Southwestern part of the Japan Sea. Earth Planet. Sci. Lett. 85, 289–301.

Otofuji, Y.I., Matsuda, T., Nohda, S., 1985. Paleomagnetic evidence for the Miocene counter-clockwise rotation of Northeast Japan—Rifting process of the Japan Arc. Earth Planet. Sci. Lett. 75, 265–277.

Oyaizu, A., Kiminami, K., 2004. Provenance changes of the late cretaceous to early Paleogene Shimanto Supergroup in Western Shikoku, and its significance. J. Geol. Soc. Jpn. 110, 403–416.

Oyaizu, A., Miura, K., Tanaka, T., Hayashi, H., Kiminami, K., 2002. Geology and radiolarian ages of the Shimanto supergroup, Western Shikoku, Southwest Japan. J. Geol. Soc. Jpn. 108, 701–720.

Pallares, C., Maury, R.C., Bellon, H., Royer, J.Y., Calmus, T., Aguillón-Robles, A., Cotten, J., Benoit, M., Michaud, F., Bourgois, J., 2007. Slab-tearing following ridge-trench collision: evidence from Miocene volcanism in Baja California. México. J. Volc. Geotherm. Res. 161, 95–117.

Pavlyutkin, B.I., Chekryzhov, I.Y., Petrenko, T.I., 2016. Problems of Paleogene–Neogene stratigraphy of the Zerkal'naya depression, East Sikhote Alin. Russ. J. Pac. Geol. 10, 283–298.

Petrov, O.V., Morozov, A.F., Chepkasova, T.V., Shevchenko, S.S., 2015. Geochronological Atlas–Text Book of Main Lithotecotnic Complexes of Russia. VSEGEI, St. Petersburg.

Popov, V.K., Grebennikov, A.V., 2001. New data on the age of effusive rocks in the Bogopol'skaya formation in primorye Tikhookean. Russ. J. Pac. Geol. 3, 47–54.

Popov, V.K., Chashchin, A.A., Tsutsumi, Y., Chekryzhov, I.Yu., Budnitsky, S.Yu., 2018. New geochronology data on Eocene–Oligocene volcanism of Kraskin rift-related basin (South-Western Primorye). International Research Journal 12(78), 75–78.

Raimbourg, H., Augier, R., Famin, V., Gadenne, L., Palazzin, G., Yamaguchi, A., Kimura, G., 2014. Long-term evolution of an accretionary prism: the case study of the Shimanto Belt, Kyushu, Japan. Tectonics 33, 936–959.

Ren, J., Tamaki, K., Li, S., Junxia, Z., 2002. Late Mesozoic and Cenozoic rifting and its dynamic setting in Eastern China and adjacent areas. Tectonophys. 344, 175–205.

Robinson, F.A., Bonin, B., Pease, V., Anderson, J.L., 2017. A discussion on the tectonic implications of Ediacaran late- to post-orogenic A-type granite in the Northeastern Arabian Shield, Saudi Arabia. Tectonics 36, 582–600.

Saito, M., 2008. Rapid evolution of the Eocene accretionary complex (Hyuga Group) of the Shimanto terrane in Southeastern Kyushu. Southwestern Japan. Isl. Arc 17, 242–260.

Sakhno, V., Kovalenko, S., 2018. Igneous complexes of the Orochenka Caldera of the East Sikhote-Alin belt: U–Pb (SHRIMP) age, trace and rare earth element composition, and Au–Ag mineralization. Dokl. Earth Sci. 479, 420–424.

Sakhno, V.G., 2001. Late Mesozoic–Cenozoic Continental Volcanism of East Asia. Dal'nauka, Vladivostok.

Sakhno, V.G., Rostovskii, F.I., Alenicheva, A.A., 2010. U-Pb isotope dating of igneous complexes from the milogradovo gold-silver deposit (Southern Primor'e). Dokl. Earth Sci. 433, 879–886.

Seton, M., Müller, R.D., Zahirovic, S., Gaina, C., Torsvik, T., Shephard, G., Talsma, A., Gurnis, M., Turner, M., Maus, S., 2012. Global continental and ocean basin reconstructions since 200 Ma. Earth-Sci. Rev. 113, 212–270.

Seton, M., Flament, N., Whittaker, J., Müller, R.D., Gurnis, M., Bower, D.J., 2015. Ridge subduction sparked reorganization of the Pacific plate-mantle system 60–50 million years ago. Geophys. Res. Lett. 42, 1732–1740.

Shibata, T., Orihashi, Y., Kimura, G., Hashimoto, Y., 2008. Underplating of mélange evidenced by the depositional ages: U–Pb dating of zircons from the Shimanto accretionary complex. Southwest Japan. Isl. Arc 17, 376–393.

Sun, S.S., Mcdonough, W.F., 1989. Chemical and isotopic systematics of oceanic basalts: Implications for mantle composition and processes. In: Saunders, A.D., Norry, M.J. (Eds.), Magmatism in the Ocean Basins. Geological Society of London Special Publication, London, pp. 313–345.

Taira, A., 2001. Tectonic evolution of the Japanese island arc system. Annu. Rev. Earth Planet. Sci. 29, 109–134.

Taira, A., Tashiro, M., 1987. Late Paleozoic and Mesozoic accretion tectonics in Japan and Eastern Asia. In: Taira, A., Tashiro, M. (Eds.), Historical Biogeogrphy and Plate Tectonic Evolution of Japan and Eastern Asia. Terra Scientific Publishing, Tokyo, pp. 1–43.

Taira, A., Katto, J., Tashiro, M., Okamura, M., Kodama, K., 1988. The Shimanto Belt in Shikoku, Japan: evolution of cretaceous to Miocene accretionary prism. Mod. Geol. 12, 5–16.

Takagi, T., 2004. Origin of magnetite-and ilmenite-series granitic rocks in the Japan arc. Am. J. Sci. 304, 169–202.

Tang, J., Xu, W., Niu, Y., Wang, F., Ge, W., Sorokin, A.A., Chekryzhov, I.Y., 2016. Geochronology and geochemistry of late Cretaceous–Paleocene granitoids in the Sikhote-Alin Orogenic Belt: petrogenesis and implications for the oblique subduction of the paleo-Pacific plate. Lithos 266, 202–212.

Tsuchiya, N., Suzuki, S., Kimura, J.I., Kagami, H., 2005. Evidence for slab melt/mantle reaction: petrogenesis of early cretaceous and Eocene high-Mg andesites from the Kitakami Mountains, Japan. Lithos 79, 179–206.

Tsutsumi, Y., Yokoyama, K., Kasatkin, S.A., Golozubov, V.V., 2016. Ages of igneous rocks in the Southern part of Primorye, Far East Russia. Mem. Natl. Mus. Nat. Sci. 51, 71–78.

Ueda, H., 2016. Hokkaido. In: Moreno, T., Wallis, S., Kojima, T., Gibbons, W. (Eds.), The Geology of Japan. Geol. Soc, London, pp. 201–222.

Utkin, V.P., 2013. Shear structural paragenesis and its role in continental rifting of the East Asian margin. Russ. J. Pac. Geol. 7, 167–188.

Uyeda, S., Miyashiro, A., 1974. Plate tectonics and the Japanese Islands: a synthesis. Geol. Soc. Am. Bull. 85, 1159–1170.

Vaes, B., Van Hinsbergen, D.J.J., Boschman, L.M., 2019. Reconstruction of subduction and back-arc spreading in the NW Pacific and Aleutian basin: clues to causes of cretaceous and Eocene plate reorganizations. Tectonics 38, 1367–1413.

Wakita, K., 2013. Geology and tectonics of Japanese islands: a review–the key to understanding the geology of Asia. J. Asian Earth Sci. 72, 75–87.

Wang, G., Li, S., Wu, Z., Suo, Y., Guo, L., Wang, P., 2018. Early Paleogene strike-slip transition of the Tan-Lu fault zone across the Southeast Bohai Bay basin: constraints from fault characteristics in its adjacent basins. Geol. J. 54, 835–849.

Wang, Z., Yang, H., Ge, W., Bi, J., Zhang, Y., Xu, W., 2016. Discovery and geological significance of the Eocene granodiorites in the Sanjiang basin, NE China: evidence from zircon U-Pb chronology, geochemistry and Sr-Nd-Hf isotopes. Acta Petrol. Sin. 32, 1823–1838.

Weigand, P.W., Savage, K.L., Nicholson, C., 2002. The Conejo volcanics and other Miocene volcanic suites in Southwestern California. In: Barth, A. (Ed.), Contributions to Crustal Evolution of the Southwestern United States. Geol. Soc. of Am. Spec. Pap, Boulder, Colorado, pp. 187–204.

Whalen, J.B., Currie, K.L., Chappell, B.W., 1987. A-type granites: geochemical characteristics, discrimination and petrogenesis. Contrib. Mineral. Petrol. 95, 407–419.

Whittaker, J.M., Müller, R.D., Leitchenkov, G., Stagg, H., Sdrolias, M., Gaina, C., Goncharov, A., 2007. Major Australian-Antarctic plate reorganization at Hawaiian-Emperor bend time. Science 318, 83–86.

Wu, J.T.J., Wu, J., 2019. Izanagi-Pacific ridge subduction revealed by a 56 to 46 Ma magmatic gap along the Northeast Asian margin. Geology 47, 953–957.

Yakushiji, A., Kamei, A., Shibata, T., 2012. Igneous activity forming hybrid rocks and leucogranites in the Obara area, San'in zone, Southwest Japan. J. Geol. Soc. Jpn. 118, 20–38.

Yamamoto, S., Senshu, H., Rino, S., Omori, S., Maruyama, S., 2009. Granite subduction: arc subduction, tectonic erosion and sediment subduction. Gondwana Res. 15, 443–453.

Zhao, P., Jahn, B.M., Xu, B., 2017. Elemental and Sr-Nd isotopic geochemistry of cretaceous to early Paleogene granites and volcanic rocks in the Sikhote-Alin orogenic belt (Russian Far East): implications for the regional tectonic evolution. J. Asian Earth Sci. 146, 383–401.

Zhao, P., Alexandrov, I., Jahn, B.M., Ivin, V., 2018. Timing of Okhotsk Sea plate collision with Eurasia plate: Zircon U-Pb age constraints from the Sakhalin Island, Russian Far East. J. Geophys. Res. Solid Earth 123, 8279–8293.

Zharov, A.E., 2004. Accretionary tectonics and geodynamics of Southern Sakhalin. Geotectonics 38, 277–293.